

Unified Theory of Characteristic Modes

Mats Gustafsson, *Senior Member, IEEE*, Lukas Jelinek,
Kurt Schab, *Member, IEEE*, and Miloslav Capek, *Senior Member, IEEE*

Abstract—A unification of characteristic mode decomposition for all method-of-moment formulations of field integral equations describing free-space scattering is derived. The work is based on an algebraic link between impedance and transition matrices, the latter of which was used in early definitions of characteristic modes and is uniquely defined for all scattering scenarios. This also makes it possible to extend the known application domain of characteristic mode decomposition to any other frequency-domain solver capable of generating transition matrices, such as finite difference or finite element methods. The formulation of characteristic modes using a transition matrix allows for the decomposition of induced currents and scattered fields from arbitrarily shaped objects, providing high numerical dynamics and increased stability, removing the issue of spurious modes, offering good control of convergence, and significantly simplifying modal tracking. Algebraic properties of the transition matrix are utilized to show that characteristic mode decomposition of lossy objects fails to deliver orthogonal far fields. All aforementioned properties and steps are demonstrated on several numerical examples for both surface- and volume-based method-of-moment formulations.

Index Terms—Antenna theory, eigenvalues and eigenfunctions, computational electromagnetics, characteristic modes, scattering, method of moments, T-matrix method.

I. INTRODUCTION

CHARACTERISTIC modes [1], [2] are established as a useful tool for antenna analysis and synthesis [3], [4]. The number and diversity of applications benefiting from this technique grows rapidly [5] and characteristic mode decomposition is implemented in many contemporary electromagnetic simulation tools based on integral equations. Despite this growth and widespread use, there are still unresolved theoretical issues, namely, the unique and consistent definition of the characteristic decomposition for material bodies [6], eigentrace tracking [7], and a problematic convergence of current expansion into characteristic currents for localized sources [8], [9].

The original definition of the characteristic mode decomposition was proposed in [10] and rigorously postulated in [1], [11] for use in scattering theory. Because this formulation is fundamentally based on scattering, it lacks many of the

ambiguities and numerical issues often observed in cases when characteristic modes are used to describe antenna problems. However, this original formulation is rarely used in contemporary work on characteristic modes due to its need for transition matrix data [12], [13] which is not commonly available in commercial electromagnetics solvers. Rather, it is the formulation of characteristic modes based on impedance operators [2], [14] proposed later on by Harrington and Mautz that is predominantly implemented in both commercial and academic tools due to its close connection to the method of moments (MoM) [15], [16]. This formulation was, however, proposed phenomenologically based on its equivalence to scattering-based formulations in the case of perfectly conducting (PEC) structures [2]. Hence, as is discussed further in this work, many of the previously mentioned issues related to unambiguous definitions of modes, tracking, and convergence stem from the use of impedance, rather than scattering, operator formulations of characteristic modes. For example, the ambiguities in defining characteristic modes for material bodies arise from the fact that the nature of the impedance matrix, and its decomposition, inherently depends on what type of MoM is utilized [17]–[21]. This leads to multiple, sometimes conflicting, formulations; their justification, however, requires comparison with the original scattering-based definition of characteristic modes.

The question addressed in this paper is whether the scattering- and impedance-based formulations can be inter-linked, *i.e.*, whether the transition matrix can be expressed in terms of the impedance matrix and decomposed in a basis of outgoing waves. This algebraic link is obtained utilizing a projection matrix [22] mapping basis functions representing current densities on arbitrary objects [23] onto a set of spherical vector waves [12].

Thanks to the direct link between the impedance and transition matrices, the physical and algebraic properties of the latter are employed to demonstrate that, for lossy scatterers, it is in general not possible to acquire orthogonal far fields and simultaneously diagonalize the matrix used for the decomposition. This observation applies to all previous works attempting to define characteristic modes for lossy objects, *e.g.*, [24].

The proposed formulation is shown to be unique to all MoM formulations¹, and, thanks to the properties of the transition matrix, many ambiguities and numerical issues are resolved. In contrast to impedance-based formulations, the transition matrix construction of characteristic modes does not exhibit issues related to spurious modes [28]. For specific geometries, the numerical dynamics of the proposed scattering-based decomposition is considerably higher than impedance-based

Manuscript received June 10, 2022; revised June 10, 2022. This work was supported by the Swedish Research Council (2017-04656) and Czech Science Foundation under project No. 21-19025M.

M. Gustafsson is with Lund University, Lund, Sweden (e-mail: mats.gustafsson@eit.lth.se).

L. Jelinek and M. Capek are with the Czech Technical University in Prague, Prague, Czech Republic (e-mails: {lukas.jelinek; miloslav.capek}@fel.cvut.cz).

K. Schab is with the Santa Clara University, Santa Clara, USA (e-mail: kschab@scu.edu).

Color versions of one or more of the figures in this paper are available online at <http://ieeexplore.ieee.org>.

Digital Object Identifier XXX

¹For example, electric field integral equation for either PEC (surface), material (volumetric) obstacles [18], or PMCHWT formulation [25]–[27] can be utilized.

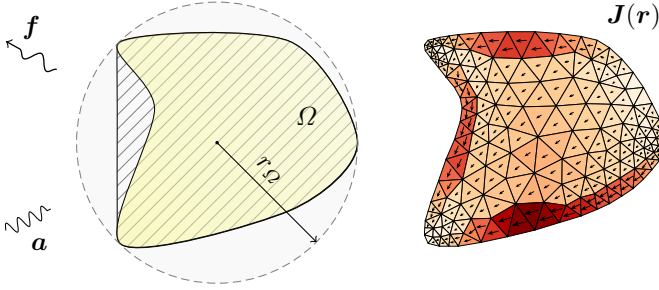


Fig. 1. Left: Schematic depiction of a scatterer Ω placed in the smallest circumscribing sphere of radius r_Ω . Electromagnetic quantities are represented outside the circumscribing sphere in the basis of spherical vector waves with expansion coefficients collected in vectors \mathbf{a} (regular waves) and \mathbf{f} (outgoing waves). The characteristic modes are expressed as specific vectors \mathbf{f}_n . Hatched region represents the inner part of the convex hull of the scatterer. Right: The dominant characteristic current of the scatterer Ω made of perfect electric conductor, electrical size $kr_\Omega = 1$.

solutions while also being considerably faster, as the problem is reduced to an ordinary eigenvalue problem of smaller size.

Decomposition via ordinary eigenvalue problems involving matrices with favorable algebraic properties also simplifies modal tracking [29]–[33], a challenging post-processing step required both for visual inspection of the eigentraces [7] (characteristic numbers parameterized by frequency) or for interpretation of physical properties of characteristic modes [33], [34]. The tracking procedure utilized in this paper operates natively over far fields and utilizes knowledge of poles in the complex plane. As a result, the procedure is computationally inexpensive, simple, and gives excellent results both in precision and in terms of the low number of frequency samples needed to reconstruct smooth, broadband eigentraces.

Because the method examined here utilizes the transition matrix, it is not dependent on a particular numerical method [35]. Rather, any method capable of delivering transition matrix data can be used. This includes both methods based on integral equations (apart from MoM, *e.g.*, discrete dipole approximation [36]) and methods based on differential equations (*e.g.*, finite element method [37], [38], finite difference frequency-domain method [39]). Consequently, characteristic mode theory becomes a general frequency-domain technique which can be implemented in a variety of electromagnetic simulators, independent of a particular numerical method.

II. EXPANSION OF ELECTROMAGNETIC FIELDS INTO SPHERICAL VECTOR WAVES

An essential part of the proposed method is the expansion of electromagnetic fields into spherical vector waves [12], [40]. Consider equivalent [41] electric and magnetic current densities \mathbf{J}^e and \mathbf{J}^m radiating in free space² [41] confined to a scatterer Ω giving rise to scattered electric and magnetic fields \mathbf{E}_s and \mathbf{H}_s , see Fig. 1. Assume further that we are only interested in studying fields at points outside of a sphere centered at the origin and circumscribing the support region Ω , *i.e.*, $|\mathbf{r}| > r_\Omega$. Under these assumptions, expansion of the

scattered fields into spherical vector waves is possible via

$$\begin{aligned} \mathbf{E}_s(\mathbf{r}) &= k\sqrt{Z} \sum_{\alpha} f_{\alpha} \mathbf{u}_{\alpha}^{(4)}(k\mathbf{r}) \\ \mathbf{H}_s(\mathbf{r}) &= j\frac{k}{\sqrt{Z}} \sum_{\alpha} f_{\alpha} \mathbf{u}_{\alpha}^{(4)}(k\mathbf{r}), \end{aligned} \quad (1)$$

where $\mathbf{u}_{\alpha}^{(p)}(k\mathbf{r})$ are spherical vector waves [12, Chap. 7], k is the free-space wavenumber, Z is the free-space impedance and time-harmonic fields³ are assumed. The superindex $p = 1$ denotes Bessel functions of the first kind (later associated with incident fields $\mathbf{E}_i, \mathbf{H}_i$ due to sources external to the region Ω), while $p = 4$ denotes Hankel functions of the second kind (associated with scattered fields $\mathbf{E}_s, \mathbf{H}_s$ due to the sources \mathbf{J}^e and \mathbf{J}^m within Ω). A bar over the index α denotes a dual index which interchanges the roles of TE and TM waves for divergence-free fields [12, Chap. 7.2].

Because the current densities \mathbf{J}^e and \mathbf{J}^m radiate in free space, it is also possible to express the scattered fields \mathbf{E}_s and \mathbf{H}_s using the free-space dyadic Green's function [42]

$$\mathbf{G}(\mathbf{r}_1, \mathbf{r}_2) = \left(\mathbf{1} + \frac{1}{k^2} \nabla \nabla \right) \frac{e^{-jk|\mathbf{r}_1 - \mathbf{r}_2|}}{4\pi |\mathbf{r}_1 - \mathbf{r}_2|} \quad (2)$$

as

$$\begin{aligned} \mathbf{E}_s &= \mathbf{E}_s^e + \mathbf{E}_s^m = -jZk\mathcal{L}\{\mathbf{J}^e\} - \mathcal{K}\{\mathbf{J}^m\} \\ \mathbf{H}_s &= \mathbf{H}_s^e + \mathbf{H}_s^m = \mathcal{K}\{\mathbf{J}^e\} - j\frac{k}{Z}\mathcal{L}\{\mathbf{J}^m\} \end{aligned} \quad (3)$$

where the linear operators \mathcal{L} and \mathcal{K} are defined as

$$\begin{aligned} \mathcal{L}\{\mathbf{J}\}(\mathbf{r}_1) &= \int_{\Omega} \mathbf{G}(\mathbf{r}_1, \mathbf{r}_2) \cdot \mathbf{J}(\mathbf{r}_2) dV_2 \\ \mathcal{K}\{\mathbf{J}\}(\mathbf{r}_1) &= \nabla_1 \times \mathcal{L}\{\mathbf{J}\}(\mathbf{r}_1). \end{aligned} \quad (4)$$

An algebraic connection between the scattered field terms in (1) and the operator form in (3) is given by the expansion of the dyadic Green's function into spherical vector waves [12], [40], [43]

$$\mathbf{G}(\mathbf{r}_1, \mathbf{r}_2) = -jk \sum_{\alpha} \mathbf{u}_{\alpha}^{(4)}(k\mathbf{r}_1) \mathbf{u}_{\alpha}^{(1)}(k\mathbf{r}_2), \quad (5)$$

where, per earlier assumptions, the observation location \mathbf{r}_1 is outside of the source region, *i.e.*, $|\mathbf{r}_1| > |\mathbf{r}_2|$. Expanding the current densities using a suitable set of real-valued basis functions $\{\psi_i\}$ as

$$\mathbf{J}^e(\mathbf{r}) \approx \sum_i I_i^e \psi_i(\mathbf{r}), \quad \mathbf{J}^m(\mathbf{r}) \approx \sum_i I_i^m \psi_i(\mathbf{r}), \quad (6)$$

the relation between the formulations (1) and (3) can be written as

$$\mathbf{f}^e = -\mathbf{U}_1 \mathbf{I}^e \quad \text{and} \quad \mathbf{f}^m = j\bar{\mathbf{U}}_1 \mathbf{I}^m, \quad (7)$$

²Throughout this work, *free space* denotes an infinite space filled by homogeneous, isotropic, and lossless material.

³Throughout this work, the time convention $\exp\{j\omega t\}$ is assumed, where $j = \sqrt{-1}$ is the imaginary unit and ω is the angular frequency.

where the matrices \mathbf{U}_1 and $\bar{\mathbf{U}}_1$ are defined⁴ as

$$\begin{aligned} \mathbf{U}_1 &= k\sqrt{Z} \left[\int_{\Omega} \mathbf{u}_{\alpha}^{(1)}(kr) \cdot \boldsymbol{\psi}_i(\mathbf{r}) dV \right] \\ \bar{\mathbf{U}}_1 &= \frac{k}{\sqrt{Z}} \left[\int_{\Omega} \mathbf{u}_{\alpha}^{(1)}(kr) \cdot \boldsymbol{\psi}_i(\mathbf{r}) dV \right], \end{aligned} \quad (8)$$

with the interpretation of being projections of regular and real-valued spherical vector waves onto the chosen basis functions $\{\boldsymbol{\psi}_i\}$ [22]. Analogously to relation (3), the expansion coefficients \mathbf{f} in (1) are given as the sum of contributions \mathbf{f}^e and \mathbf{f}^m from electric and magnetic current densities, respectively.

The equivalent current densities \mathbf{J}^e and \mathbf{J}^m may be induced by an incident field with sources located outside of the sphere circumscribing the scatterer. Within this circumscribing sphere, such an incident field may be expanded as

$$\begin{aligned} \mathbf{E}_i(\mathbf{r}) &= k\sqrt{Z} \sum_{\alpha} a_{\alpha} \mathbf{u}_{\alpha}^{(1)}(kr) \\ \mathbf{H}_i(\mathbf{r}) &= j \frac{k}{\sqrt{Z}} \sum_{\alpha} a_{\alpha} \mathbf{u}_{\alpha}^{(1)}(kr). \end{aligned} \quad (9)$$

Within the aforementioned notation, a scattering obstacle's transition⁵ matrix \mathbf{T} relates the coefficients of regular and outgoing spherical waves as [12, Chap. 7.8]

$$\mathbf{f} = \mathbf{T}\mathbf{a}. \quad (10)$$

Alternatively, decomposing regular spherical waves into outgoing and in-going waves leads to a scattering matrix

$$\mathbf{S} = \mathbf{1} + 2\mathbf{T} \quad (11)$$

relating the associated sets of coefficients [12, Chap. 7.8], where $\mathbf{1}$ denotes an identity matrix.

By virtue of the orthogonality of spherical vector waves over spherical surfaces, orthogonality and radiation properties of scattered fields of the form of (1) may be written in terms of their associated expansion vector \mathbf{f} . Specifically, the cycle mean power P_{rad} , radiated by a field described by the vector \mathbf{f} , reads

$$P_{\text{rad}} = \frac{1}{2} \mathbf{f}^H \mathbf{f} = \frac{1}{2Z} \int_{4\pi} \mathbf{F}^*(\hat{\mathbf{r}}) \cdot \mathbf{F}(\hat{\mathbf{r}}) d\Omega, \quad (12)$$

where the superscript $*$ denotes complex conjugation, the integration is carried out over the full solid angle, and the vector

$$\mathbf{F}(\hat{\mathbf{r}}) = \lim_{r \rightarrow \infty} r e^{jkr} \mathbf{E}(\mathbf{r}) \quad (13)$$

denotes the electric far field. Here the vector $\hat{\mathbf{r}}$ represents a unit vector in the radial direction. Similarly, two far fields described by the vectors \mathbf{f}_a and \mathbf{f}_b are orthogonal if

$$\frac{1}{2} \mathbf{f}_a^H \mathbf{f}_b = \frac{1}{2Z} \int_{4\pi} \mathbf{F}_a^*(\hat{\mathbf{r}}) \cdot \mathbf{F}_b(\hat{\mathbf{r}}) d\Omega = 0. \quad (14)$$

TABLE I
CLASSIFICATION OF CHARACTERISTIC NUMBERS AND ANGLES
DEPENDING ON THEIR PHYSICAL NATURE.

	λ_n	t_n	s_n	ϕ_n	α_n
external res.	0	-1	-1	$\pm\pi$	π
internal res.	$\pm\infty$	0	1	0	$\pi \mp \pi/2$
capacitive	< 0	$\text{Im}\{t_n\}, \text{Im}\{s_n\} < 0$		$(-\pi, 0)$	$(\pi, 3\pi/2)$
inductive	> 0	$\text{Im}\{t_n\}, \text{Im}\{s_n\} > 0$		$(0, \pi)$	$(\pi/2, \pi)$

III. CHARACTERISTIC MODES OF LOSSLESS SCATTERERS

Characteristic modes for lossless scatterers were originally defined as eigenvectors of scattering [10, Chap. 9] or transition (perturbation) [1] matrices. In the latter case, characteristic modes have the interpretation of being vectors of incident or scattered field expansion coefficients which map to scaled versions of themselves through the transition matrix [1], *i.e.*,

$$\mathbf{T}\mathbf{f}_n = t_n \mathbf{f}_n. \quad (15)$$

With \mathbf{f}_n interpreted as describing a characteristic scattered field, the corresponding characteristic incident field \mathbf{a}_n is given by (10) and (15) as

$$\mathbf{a}_n = t_n^{-1} \mathbf{f}_n. \quad (16)$$

The eigenvalues t_n lie on a circle in a complex plane [12, Chap. 7] and can be mapped onto the real axis by defining characteristic numbers $\lambda_n \in \mathbb{R}$ [2], [11] as

$$t_n = -\frac{1}{1 + j\lambda_n}, \quad (17)$$

see Fig. 2. Characteristic numbers can be interpreted as the ratio between the imaginary and real parts of the modal complex power

$$P_{c,n} = -\mathbf{f}_n^H \mathbf{a}_n / 2 = -t_n^{-1} P_{\text{rad},n} \quad (18)$$

interchanged between the modal incident field \mathbf{a}_n and the scatterer, see Appendix A, which together with (17) reveals a similar identity with the eigenvalues t_n

$$\lambda_n = \frac{\text{Im}\{P_{c,n}\}}{\text{Re}\{P_{c,n}\}} = -\frac{\text{Im}\{t_n\}}{\text{Re}\{t_n\}}. \quad (19)$$

The eigenvalue magnitude $|t_n|$ is commonly referred to as characteristic modal significance [44]

$$|t_n| = \frac{1}{|1 + j\lambda_n|}, \quad (20)$$

as it is related to the relative significance of each characteristic mode within an expansion of a total scattered field.

For lossless scatterers, \mathbf{T} is a normal matrix (see Appendix A) giving rise to eigenvectors \mathbf{f}_n that are orthogonal [11], may be normalized as

$$\mathbf{f}_m^H \mathbf{f}_n = \delta_{mn}, \quad (21)$$

and can be chosen to be real valued for reciprocal $\mathbf{T} = \mathbf{T}^T$ obstacles. By (14), this implies orthogonal characteristic far

⁴In the reference [22] these matrices were denoted by \mathbf{S} . In this paper, symbol \mathbf{U} is used instead and the symbol \mathbf{S} is used for scattering matrices.

⁵Notice that in early texts on characteristic modes, such as [2], [11], this matrix is called a perturbation operator.

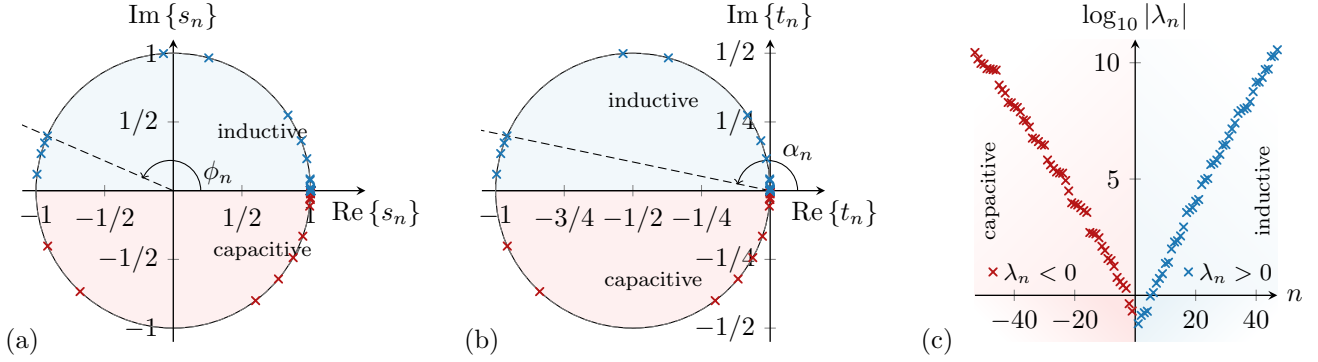


Fig. 2. (panel a, panel b) Eigenvalues s_n and t_n as products of eigenvalue decomposition (22), (15). (panel c) characteristic numbers λ_n as products of relation (17) or generalized eigenvalue decomposition (25). All eigenvalues were evaluated for a perfectly conducting rectangular plate of aspect ratio 2 : 1, and electrical size $kr_\Omega = 5$.

fields. These properties can also be observed via decomposition of the scattering matrix

$$\mathbf{S}\mathbf{f}_n = s_n \mathbf{f}_n = e^{j\phi_n} \mathbf{f}_n \quad (22)$$

where⁶ $\phi_n = 2 \arctan(\lambda_n^{-1})$ and the scattering matrix \mathbf{S} for lossless objects is unitary [45, Chap. 4], see Appendix A. By (22), the eigenvalues s_n of the scattering matrix are related to those of the transition matrix t_n by

$$s_n = 1 + 2t_n. \quad (23)$$

Graphical representation of the relations between eigenvalues s_n , t_n and characteristic numbers λ_n is given in Fig. 2 while Table III lists values and regions of physical interest, namely the scattering (external) resonances [11] at which the corresponding modes contribute significantly to scattering, scattering nulls (internal resonances) [11] at which the corresponding modes makes no contribution to scattering, and regions of capacitive/inductive modal behavior which are characterized by an excess of stored electric/magnetic energy. Table III also shows values of characteristic eigenangle α_n , introduced in [11] and later in [46], which is given by $\alpha_n = \pi - \arctan(\lambda_n)$ and measures the angle of eigenvalue t_n , see Fig. 2.

The eigenvectors \mathbf{a}_n , proportional to the vectors \mathbf{f}_n via (16), can be interpreted as orthogonal incident field configurations maximizing the ratio between radiated (12) and incident power

$$\max_{\mathbf{a}_n} \frac{\mathbf{a}_n^H \mathbf{T}^H \mathbf{T} \mathbf{a}_n}{\mathbf{a}_n^H \mathbf{a}_n} \quad \text{with } \mathbf{a}_n^H \mathbf{a}_m = 0 \quad \forall m < n, \quad (24)$$

where $\mathbf{a}_n^H \mathbf{a}_n$ is the incident power in the scattering matrix description (11). The connection between (15) and the Rayleigh quotient [47] in (24) follows from $\mathbf{T}^H \mathbf{T} \mathbf{a}_n = t_n \mathbf{T}^H \mathbf{a}_n = |t_n|^2 \mathbf{a}_n$ for lossless cases, where vector \mathbf{a} is real-valued, see Appendix A. This interpretation of characteristic modes could be used as an alternative physics-based definition of characteristic modes.

In the form of (15), the evaluation of characteristic modes was bound to cases where the transition matrix was known

⁶This choice is not unique and was made to obtain vanishing angle $\phi_n = 0$ for insignificant characteristic values $|\lambda_n| \rightarrow \infty$, $|t_n| \rightarrow 0$.

analytically [1] or cases which could be addressed via the Null-field method [12], [48], *i.e.*, mostly to spheroidal bodies. This difficulty was overcome by Harrington and Mautz [2], [16] who used MoM formulations of field integral equations to express characteristic modes for bodies of arbitrary shape. In their formulation, characteristic modes of perfectly conducting obstacles described by the electric field integral equation (EFIE) were eigensolutions to a generalized eigenvalue problem

$$\mathbf{Z}^{ee} \mathbf{I}_n^e = (1 + j\lambda_n) \text{Re} \{ \mathbf{Z}^{ee} \} \mathbf{I}_n^e, \quad (25)$$

where \mathbf{Z}^{ee} is the system matrix of the discretized electric field integral equation [15]

$$\mathbf{Z}^{ee} \mathbf{I}^e = \mathbf{V}^e, \quad (26)$$

with \mathbf{V}^e containing the incident electric field expansion coefficients (defined below in (29)). Through the relation

$$P_{c,n} = \frac{1}{2} (\mathbf{I}_n^e)^H \mathbf{V}_n^e = (1 + j\lambda_n) P_{\text{rad},n}, \quad (27)$$

the formulation in (25) also clearly presents the connection between the characteristic value λ_n and the power ratio in (19). This formulation of characteristic modes was later extended to lossless penetrable scatterers using volume [24] and surface [27] formulations.

The formulation of characteristic modes based on field integral equations brings computational flexibility, nevertheless it also allows for spurious (and unwanted) solutions [49] which are not present in the original formulation (15). Different possibilities in formulating field integral equations [50] also make it difficult to identify the radiation operator that should be put on the RHS of (25) in order to maintain far-field orthogonality. In the following section, a proposal is made to remove these issues, keeping the computational capabilities of field integral equations, while also returning to the original definition of characteristic modes in (15).

IV. EVALUATION OF CHARACTERISTIC MODES USING TRANSITION MATRIX

Here we formulate a connection between the method-of-moments impedance matrix and the transition matrix \mathbf{T} .

The goal of this connection is to establish a procedure for evaluating characteristic modes using the transition matrix formulation in (15) while maintaining the flexibility afforded by impedance-based formulations, such as (25), particularly regarding the analysis of arbitrarily shaped obstacles. The procedure is presented on a MoM formulation of field integral equations for penetrable bodies based on the surface equivalence principle (*e.g.*, PMCHWT, Poggio-Miller-Chang-Harrington-Wu-Tsai and Müller formulations) [25]–[27], [51]. Adaptations to other formulations are shown in Appendix B.

In these formulations, the MoM system describing the scattering scenario in Section II reads [27]

$$\begin{bmatrix} \mathbf{Z}^{ee} & j\mathbf{Z}^{em} \\ j\mathbf{Z}^{me} & \mathbf{Z}^{mm} \end{bmatrix} \begin{bmatrix} \mathbf{I}^e \\ j\mathbf{I}^m \end{bmatrix} = \begin{bmatrix} \mathbf{V}^e \\ j\mathbf{V}^m \end{bmatrix}, \quad (28)$$

where the excitation vectors \mathbf{V}^e and \mathbf{V}^m represent the incident electric field \mathbf{E}^i and incident magnetic field \mathbf{H}^i via

$$\begin{aligned} \mathbf{V}_n^e &= \int_{\Omega} \mathbf{E}^i(\mathbf{r}) \cdot \psi_n(\mathbf{r}) dS \\ \mathbf{V}_n^m &= \int_{\Omega} \mathbf{H}^i(\mathbf{r}) \cdot \psi_n(\mathbf{r}) dS, \end{aligned} \quad (29)$$

respectively, and different components of the partitioned system matrix refer to inner products between basis functions and their projections through the \mathcal{K}, \mathcal{L} operators (4) in the interior and exterior regions, see Appendix B. For brevity, the partitioned system (28) is written as

$$\mathbf{Z}\mathbf{I} = \mathbf{V}, \quad (30)$$

where it is assumed that the impedance matrix \mathbf{Z} is invertible.

Employing the field expansion (9), and assuming that sources of the incident field are external to the convex hull of the scatterer [52] (see Fig. 1 and related discussion in Section IX-C), it is possible to write the incident fields in terms of the regular wave expansion coefficients in (9) as

$$\mathbf{V} = \mathbf{U}^T \mathbf{a}, \quad (31)$$

where

$$\mathbf{U} = [\mathbf{U}_1 \quad -\bar{\mathbf{U}}_1]. \quad (32)$$

Additionally, by (7), the radiated fields produced by the electric and magnetic currents may be expressed in terms of the outgoing spherical wave expansion coefficients in (1) as

$$\mathbf{f} = -\mathbf{U}\mathbf{I}. \quad (33)$$

Left multiplying (30) by $-\mathbf{U}\mathbf{Z}^{-1}$, and substituting from (31) and (33) results in

$$\mathbf{T} = -\mathbf{U}\mathbf{Z}^{-1}\mathbf{U}^T, \quad (34)$$

which in the simpler form with only \mathbf{Z}^{ee} was obtained in [53]–[56], see also [57], [58]. When the above expression is used to express the transition matrix, the eigenvalue problem in (15) yields a formulation of characteristic modes with both the computational advantages of the impedance-based description

together with the robust and original transition matrix definition. Relations analogous to (34) for other common field-integral formulations⁷ are given in Appendix B.

An apparent drawback of the aforementioned formulation involving a combination of (15) and (34) is that characteristic eigenvectors are given in terms of the scattered field expansion coefficients \mathbf{f} . This can be resolved by realizing that, by (16), an eigenvector \mathbf{f}_n corresponds to a particular excitation \mathbf{a}_n . An analogous relation holds for the current eigenvectors \mathbf{I}_n , which are linked to specific excitations through (30) as

$$\mathbf{I}_n = \mathbf{Z}^{-1}\mathbf{V}_n = \mathbf{Z}^{-1}\mathbf{U}^T \mathbf{a}_n = t_n^{-1}\mathbf{Z}^{-1}\mathbf{U}^T \mathbf{f}_n, \quad (35)$$

where (31) has been used to relate the excitation vector \mathbf{V}_n with the excitation vector \mathbf{a}_n . Therefore, even when characteristic currents are desired, there is no need to solve a generalized eigenvalue problem in a form similar to (25). Rather, solving the simpler ordinary eigenvalue problem (15) is sufficient. It is also worth noting that the computation of characteristic currents \mathbf{I}_n is carried out by multiplication of eigenvectors \mathbf{f}_n with the matrix $\mathbf{Z}^{-1}\mathbf{U}^T$ which was already used to determine the transition matrix \mathbf{T} through relation (34). The evaluation of characteristic currents therefore requires only minor additional computational burden. Relation (35) shows that characteristic currents are undefined at scattering nulls characterized by vanishing eigenvalue $t_n = 0$ and infinitely large characteristic number $|\lambda_n| \rightarrow \infty$.

V. EVALUATION OF CHARACTERISTIC MODES USING CURRENTS

From (35), a generalized eigenvalue problem directly in characteristic currents may be formed which illustrates similarities and differences between the impedance-based (25) and scattering-based (15) methods for computing characteristic modes. Left multiplying (35) by the matrix \mathbf{Z} and substituting (33) for the eigenvector \mathbf{f}_n produces the generalized eigenvalue problem

$$\mathbf{Z}\mathbf{I}_n = (1 + j\lambda_n)\mathbf{R}_0\mathbf{I}_n, \quad (36)$$

where, by using $\mathbf{U}^H = \mathbf{U}^T$ for real-valued basis functions and real-valued regular spherical waves in (8), the radiation operator \mathbf{R}_0 is defined by

$$\mathbf{R}_0 = \mathbf{U}^H\mathbf{U}. \quad (37)$$

This last association is possible due to the chosen expansion into spherical waves which allows the radiated power (12) to be written as

$$P_{\text{rad}} = \frac{1}{2}\mathbf{f}^H\mathbf{f} = \frac{1}{2}\mathbf{I}^H\mathbf{U}^H\mathbf{U}\mathbf{I}, \quad (38)$$

see Appendix A. The use of (37) to define the radiation operator in the eigenvalue problem (36) is distinct from purely impedance-based characteristic mode formulations (*e.g.* [16]) in that it uniquely defines the radiation matrix \mathbf{R}_0 independently of the impedance matrix \mathbf{Z} . Hence, irrespective of the

⁷Conversion of an impedance matrix \mathbf{Z} into a transition matrix \mathbf{T} also gives a possibility to verify the correctness of the underlying impedance matrix formulation, since the matrix \mathbf{T} is unique to a given scatterer and has eigenvalues lying on a circle in the complex plane, see Fig. 2.

particular form of the impedance matrix \mathbf{Z} , the characteristic currents in (35) computed by the problem (15) are orthogonal with respect to matrix \mathbf{R}_0 for lossless scenarios and may be normalized as

$$\mathbf{I}_m^H \mathbf{R}_0 \mathbf{I}_n = \mathbf{f}_m^H \mathbf{f}_n = \delta_{mn}, \quad (39)$$

where the last equality stems from properties discussed in Section III. By virtue of (14), the above expression implies orthogonal characteristic far fields. For lossless systems, relation (35) produces characteristic currents orthogonal with respect to the impedance matrix \mathbf{Z} , *i.e.*,

$$\mathbf{I}_m^H \mathbf{Z} \mathbf{I}_n = (1 + j\lambda_n) \delta_{mn}. \quad (40)$$

VI. MODE TRACKING AND INTERPOLATION

Consider a case where the matrix $\mathbf{T}(k_q)$ is computed for a set of wavenumbers (frequencies) k_q for $q = \{1, 2, \dots, N_q\}$. At each wavenumber its eigenvalues $t_n(k_q)$ and eigenvectors $\mathbf{f}_n(k_q)$ are also calculated via (15). Modal data at each frequency are initially uncorrelated, though it is often desirable to apply modal tracking to order and associate modal quantities such that they may be interpreted as functions of frequency. Many methods have been proposed for numerical [29]–[32], [59], [60] or analytical symmetry-based [33], [61] tracking of characteristic mode quantities, however the small size of the transition matrix \mathbf{T} and the high accuracy of its corresponding characteristic mode decomposition make it exceptionally well suited for this task. This section describes different approaches for tracking and interpolation for lossless objects starting with rational approximations of scattering matrices \mathbf{S} defined in (11).

Scattering matrices can be interpolated by fitting rational functions with methods such as Nevanlinna–Pick interpolation [62] and vector fitting [63]. For that, the scattering matrix (11) must be made passive using a time shift $2r_\Omega/c$, where c denotes the speed of light. This corresponds to multiplication of the scattering matrix (11) by a phase term $\exp\{-2jk r_\Omega\}$, constructing a passive scattering matrix [64]

$$\tilde{\mathbf{S}} = \mathbf{S} e^{-2jk r_\Omega}. \quad (41)$$

The phase shifted scattering matrix may be transformed into a lossless transfer matrix [45, Chap. 4]

$$\tilde{\mathbf{H}} = (\mathbf{1} - \tilde{\mathbf{S}})^{-1} (\mathbf{1} + \tilde{\mathbf{S}}), \quad (42)$$

which is characterized by its poles located at real values of wavenumber k and its monotonically increasing imaginary part (Foster’s reactance theorem [45, Chap. 4]) for real frequencies between these poles. Quadratic forms $\tilde{h}_y(k) = -j\mathbf{y}^H \tilde{\mathbf{H}} \mathbf{y}$ with arbitrary frequency independent vectors \mathbf{y} reduce $\tilde{\mathbf{H}}$ to scalar lossless transfer functions $\tilde{h}_y(k)$ [65], which can be represented as

$$\tilde{h}_y(k) = \frac{-b_0}{k} + \sum_{m=1}^M \frac{2b_m k}{\xi_m^2 - k^2} + \frac{k}{b_\infty}, \quad (43)$$

where $\xi_m \geq 0$, $b_m \geq 0$, and M denotes the number of poles in the frequency interval $k \in (0, \infty)$. Sample points with decreasing imaginary part $\text{Im}\{\tilde{h}_y(k)\}$ identify intervals where

it is necessary to place poles ξ_m . There can also be poles outside the range of sample points and in the numerical examples in Section VIII-B a single pole in the interval (k_{N_q}, ∞) was used. Locations and residues of the poles are determined by minimizing the least squared error between the rational model (43) and values of the transfer function $\tilde{h}_y(k)$ at the sample points. It is sufficient to use vectors \mathbf{y} each having a single non-zero element (pointing to diagonal elements of matrix $\tilde{\mathbf{H}}$) together with all vectors \mathbf{y} having two complex valued non-zero elements, *e.g.*, 1 and j [65] to reconstruct the matrix $\tilde{\mathbf{H}}$. The scalar rational functions are used to synthesize a rational matrix function approximating the transfer matrix $\tilde{\mathbf{H}}$, which is used to approximate scattering and transition matrices \mathbf{S} and \mathbf{T} between the original sample points. This rational matrix function can hence be used to approximate eigenvalues s_n and t_n as well as eigenvectors \mathbf{f}_n in the frequency interval given by the sample points. However, constructing the eigencurrents \mathbf{I}_n using (35) requires additional interpolation or evaluation of the impedance matrix \mathbf{Z} at the interpolation frequency points. The rational fit works best for scatterers with narrowband resonances as illustrated in Section VIII-B and techniques described below are better for wideband resonances and modes with low modal significance $|t_n| \approx 0$.

Foster’s reactance theorem can alternatively be formulated as a monotonically decreasing phase of the scattering matrix $\tilde{\mathbf{S}}$, with the representation

$$\tilde{\mathbf{S}}(k) = \exp(j\Phi(k)) \quad (44)$$

where $\Phi(k)$ is a monotonically decreasing Hermitian matrix function⁸ and $\exp(\cdot)$ denotes the matrix exponent. These phase matrices are related to an unwrapped matrix logarithm of the phase shifted scattering matrix $\tilde{\mathbf{S}}$, similar to standard phase unwrapping for scalar phase functions. Linear interpolation of the phase matrices is also similar to an interpolation between two scattering matrices $\mathbf{S}(k_q)$ and $\mathbf{S}(k_{q+1})$ given by

$$\mathbf{S}(k_q + \nu(k_{q+1} - k_q)) = \mathbf{S}(k_q) (\mathbf{S}(k_q)^{-1} \mathbf{S}(k_{q+1}))^\nu, \quad (45)$$

with $0 \leq \nu \leq 1$, see Appendix C. This linear interpolation of the phase works well for non-resonant cases, where the phase changes slowly. The two approximations (43) and (45) are hence complementary, which calls for their combination. Construct first a rational approximation \mathbf{S}_1 of the scattering matrix based on dominant elements of matrix \mathbf{T} , *e.g.*, large diagonal elements, to capture resonances. Removing these resonances from the scattering matrix by dividing \mathbf{S} with \mathbf{S}_1 constructs a unitary matrix

$$\mathbf{S}_2 = \mathbf{S}_1^{-1} \mathbf{S} \quad (46)$$

with slower phase variation, which can be interpolated using (45). The interpolated scattering matrix is finally synthesized as $\mathbf{S}_1 \mathbf{S}_2$.

In this paper, we also use interpolation of the phase in the scalar case based on tracked modes. Tracking of the modes simplifies the matrix interpolation to scalar interpolation of

⁸Defined as having $\mathbf{I}^H \Phi(k) \mathbf{I}$ monotonically decreasing for all \mathbf{I}

each separate eigenvalue. Tracking based on maximizing correlation between each eigenvector \mathbf{f}_m at frequency k_q and eigenvectors \mathbf{f}_n at frequency k_{q+1} , *i.e.*,

$$\max_n \{ |\mathbf{f}_m(k_q)^H \mathbf{f}_n(k_{q+1})| \} \quad (47)$$

is used here. By means of (14), this corresponds to the far-field tracking procedure [32], [59].

Assuming tracked modes (47) with eigenvalues $s_n(k_q) = \exp\{j\phi_n(k_q)\}$ on a unit circle sampled at wavenumbers k_q , a phase ϕ_n wrapped to the interval $[-\pi, \pi]$ has discontinuities and is hence not suitable for interpolation. The phase ϕ_n is 2π -periodic and unwrapping is used to remove the jumps and produce a smooth function which is suitable for interpolation. Standard unwrapping by adding multiples of 2π to minimize jumps works well for sampling which is sufficiently dense to resolve all resonances, but does not work for coarse sampling. Shifting the phase according to (41) transforms eigenvalues $s_n(k)$ to a lossless scattering parameter $\tilde{s}_n(k) = s_n(k) \exp\{-2jkr_\Omega\}$ which has a monotonically decreasing phase according to Foster's reactance theorem. This approximation can be used in the unwrapping algorithm by subtracting the phase with 2π at samples with increasing $\arg(\tilde{s}_n(k_q))$, *i.e.*, the unwrapped phase is constructed to satisfy

$$\phi_n(k_p) - 2k_p r_\Omega > \phi_n(k_q) - 2k_q r_\Omega \quad \text{for } k_q > k_p. \quad (48)$$

Linear or higher-order interpolation is used to estimate phase between the sample points. This scalar interpolation can hence be used to find scattering resonances $\phi_n = -\pi + 2m\pi$ ($t_n = -1$ or $\lambda_n = 0$) for cases when the resonance frequency is not sampled, similarly to the rational fitting discussed above.

VII. CHARACTERISTIC MODES OF LOSSY SCATTERERS

A natural way of extending the theory developed in previous sections is to take into account lossy obstacles. In this section, we describe the loss of characteristic far-field orthogonality from the perspective of the properties of the transition matrix \mathbf{T} and impedance matrix \mathbf{Z} for lossy systems.

A. Normality of the Transition Matrix

The far-field orthogonality in characteristic modes for lossless systems in (21) followed from the spectral theorem which states that a matrix is unitary diagonalizable if and only if the matrix is normal [47]. Justification of the normality of the matrix \mathbf{T} for lossless systems is given in Appendix A. When losses are present, normality is generally lost, which, as shown in Appendix A, can be linked to the loss of time-reversal symmetry. Normality of the transition matrix can further be linked to specific properties of the underlying impedance matrix. Consider, for example, an impedance matrix of the form of $\mathbf{Z} = \mathbf{R}_\rho + \mathbf{R}_0 + j\mathbf{X}$ with $\text{Re}\{\mathbf{Z}\} = \mathbf{R}_\rho + \mathbf{R}_0$ and \mathbf{R}_ρ representing losses. The relation (34) can be used to rewrite $\mathbf{T}^H \mathbf{T} = \mathbf{T} \mathbf{T}^H$ as

$$\mathbf{U}(\mathbf{Z}^{-H} \mathbf{R}_0 \mathbf{Z}^{-1}) \mathbf{U}^T = \mathbf{U}(\mathbf{Z}^{-1} \mathbf{R}_0 \mathbf{Z}^{-H}) \mathbf{U}^T, \quad (49)$$

or equivalently

$$\mathbf{U}(\mathbf{Z}^{-H} \mathbf{R}_\rho \mathbf{Z}^{-1}) \mathbf{U}^T = \mathbf{U}(\mathbf{Z}^{-1} \mathbf{R}_\rho \mathbf{Z}^{-H}) \mathbf{U}^T. \quad (50)$$

Assuming further that the matrix \mathbf{R}_ρ is invertible, the inner part of relation (50) simplifies to

$$\mathbf{Z} \mathbf{R}_\rho^{-1} \mathbf{Z}^H = \mathbf{Z}^H \mathbf{R}_\rho^{-1} \mathbf{Z} \quad (51)$$

which, with $\mathbf{X} = \text{Im}\{\mathbf{Z}\}$, reduces to

$$\mathbf{R}_0 \mathbf{R}_\rho^{-1} \mathbf{X} = \mathbf{X} \mathbf{R}_\rho^{-1} \mathbf{R}_0. \quad (52)$$

This resembles a commutator relation between \mathbf{R}_0 and \mathbf{X} weighted by \mathbf{R}_ρ^{-1} . The matrices in (52) can be permuted as long as they are invertible.

Because the above relation represents a sufficient condition for normality of the transition matrix, we conclude that it is in general not possible to diagonalize the matrix \mathbf{T} of a lossy scatterer with eigenmodes having orthogonal far fields. Rather, as shown in [24], eigenmodes diagonalizing the matrix \mathbf{T} have (assuming reciprocity) a diagonal matrix of reaction products

$$\mathbf{f}_m^T \mathbf{f}_n = c_n \delta_{mn}, \quad (53)$$

where T is the matrix transpose and $|c_n| \leq 1$ assuming that modes are normalized as $\mathbf{f}_n^H \mathbf{f}_n = 1$. This nevertheless does not guarantee far-field orthogonality as defined in (14) and, in general for lossy systems we have the eigenvectors of the matrix \mathbf{T} giving

$$\mathbf{f}_m^H \mathbf{f}_n = \rho_{mn}, \quad (54)$$

with ρ_{mn} being a matrix of correlation coefficients with non-zero off-diagonal elements. Note that the magnitude squared of these coefficients correspond to the envelope correlation coefficients used to describe multiple-input multiple-output (MIMO) antenna systems [66], [67].

Losses also change the eigenvalues t_n and s_n from being restricted to the rim of the circles in Fig. 2 to also occupying their inner regions. Modes satisfying $|s_n| < 1$ are interpreted as lossy. The corresponding characteristic values (17) are then transformed from being real-valued in the lossless case to complex-valued [24] in the lossy case, with modal dissipation factor [6] being given as $\delta_n = -\text{Im}\{\lambda_n\}$. These statements follow directly from the realization that cycle mean modal lost power is given by

$$P_{\text{lost},n} = \text{Re}\{P_{c,n}\} - P_{\text{rad},n} \quad (55)$$

and therefore

$$\delta_n = \frac{P_{\text{lost},n}}{P_{\text{rad},n}} = -\text{Re}\left\{1 + \frac{1}{t_n}\right\}, \quad (56)$$

see Appendix A and (18).

B. Interpretation of Simultaneous Diagonalization

The condition in (52) is equivalent to the requirement of simultaneous diagonalization (by congruence) of three symmetric matrices \mathbf{X} , \mathbf{R}_0 , and \mathbf{R}_ρ , see [68] and Appendix D, which is not possible in most cases. However additional perspectives can be obtained by studying hypothetical cases where simultaneous diagonalization of the three matrices \mathbf{X} ,

\mathbf{R}_0 , and \mathbf{R}_ρ is possible. If such diagonalization were possible, then, the following orthogonality relations hold

$$\mathbf{I}_m^H \mathbf{R}_0 \mathbf{I}_n = \delta_{mn}, \quad (57)$$

$$\mathbf{I}_m^H \mathbf{R}_\rho \mathbf{I}_n = d_m \delta_{mn}, \quad (58)$$

$$\mathbf{I}_m^H \mathbf{X} \mathbf{I}_n = l_m \delta_{mn}. \quad (59)$$

For homogeneous dielectric bodies, the ohmic loss operator in (58) is generated by the Gramian matrix scaled by a resistivity ρ , *i.e.*, $\mathbf{R}_\rho = \text{Re}\{\rho\} \Psi$ [69]. Combining orthogonality relations (57) and (58) yields

$$\mathbf{I}_m^H (\mathbf{R}_0 + \Psi) \mathbf{I}_n = (d_m / \text{Re}\{\rho\} + 1) \delta_{mn}. \quad (60)$$

It is obvious that if characteristic modes for lossy objects would exist, their modal currents would not depend on the complex resistivity ρ , *i.e.*, they would have the same shape as for an equivalent lossless system, *e.g.*, PEC obstacles. Interestingly, this hypothesis can be confirmed for rare cases where the simultaneous diagonalization of (57)–(59) is possible, *i.e.*, for fully separable bodies [70] like a spherical shell, for which the characteristic currents are vector spherical harmonics [1], [71], and their shape is constant both in frequency and for arbitrary resistivity. Only the eigenvalues are properly rescaled. Other notable exceptions exist in cases involving obstacles with cylindrical and planar symmetries, where \mathbf{T} is diagonal (and normal) by construction [70], and in cases with dominant modes belonging to different irreducible representations of a symmetry group [33], [72] such as modes with even and odd (reflection) symmetry, see Section VIII-D.

VIII. RESULTS

This section presents the capabilities of the aforementioned methodology on selected examples, discussing the achieved numerical precision, ease of modal tracking, interpolation, and issues related to the characteristic modes of lossy scatterers.

A. Dielectric Sphere

Characteristic numbers for a dielectric sphere with relative permittivity $\varepsilon_r = 3$ are depicted in Fig. 3. Characteristic numbers are calculated using (15) and (17) in which the matrix \mathbf{T} was evaluated by (34) with the underlying impedance matrix taken from the PMCHWT formulation (solid curves) or in which matrix \mathbf{T} was evaluated analytically using the Mie series [12] (markers). Colors are used to distinguish different modes. Modes are tracked using the correlation matrix (47), which is diagonal down to numerical precision for this special case. The maximum necessary degree of spherical vector waves is estimated from [73]

$$L_{\max} = \lceil kr_\Omega + \iota \sqrt{kr_\Omega + 3} \rceil, \quad (61)$$

where the parameter ι controls the accuracy. High accuracy is needed to compute characteristic numbers with large amplitude and $\iota = 7$ was used in Fig. 3 with parameter $kr_\Omega = 5$ for the entire frequency range. This gives the maximal degree $L_{\max} = 20$ and leads to a total of $2L_{\max}(L_{\max} + 2) = 880$ spherical waves, however rotational symmetry reduces the number of independent waves

to $2L_{\max} = 40$ using a body of revolution (BoR) formulation [74].

The results show that numerically evaluated characteristic numbers agree with the analytic results over a high dynamic range [22] and that they are sorted using (47) in agreement with index-based analytic mode ordering. A comparison of current profiles numerically obtained from (35) and current profiles known analytically is shown in Fig. 4 for the electrical size $kr_\Omega = 1$. Only the dependence on the polar angle ϑ of modes independent on the azimuthal angle φ is shown for brevity. The results show that the numerically computed modes agree with the analytical modes for all considered cases.

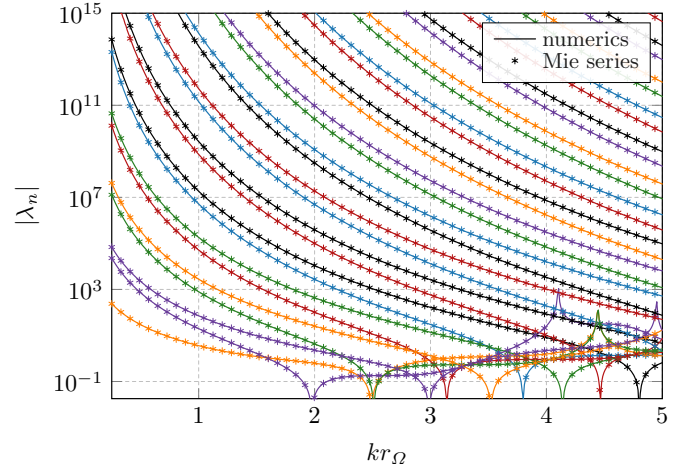


Fig. 3. Magnitude of characteristic values for a dielectric sphere with relative permittivity $\varepsilon_r = 3$ calculated using PMCHWT formulation (curves) and with analytic expressions based on Mie series (markers).

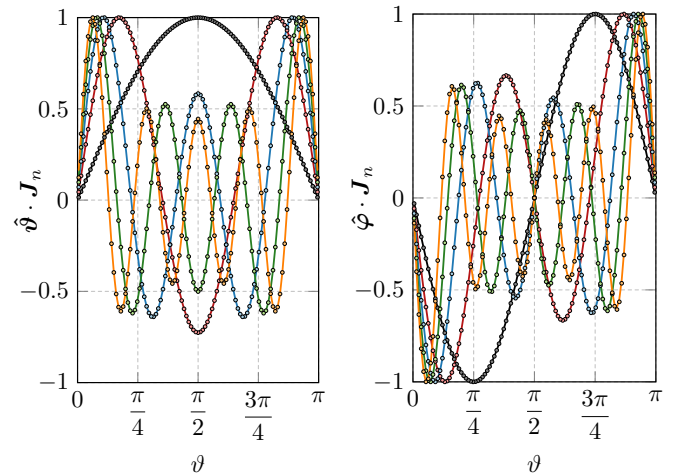


Fig. 4. Profiles of characteristic currents for the same setup as in Fig. 3 and electrical size $kr_\Omega = 1$. Solid curves correspond to numerical procedure (35), while markers show analytical result. Only modes independent on the azimuthal angle φ are shown and every second mode (even and odd) of the 20 first in Fig. 3 are shown for ϑ and φ components. For presentation purposes, peak values of modal profiles were all normalized to unity instead of using normalization (39).

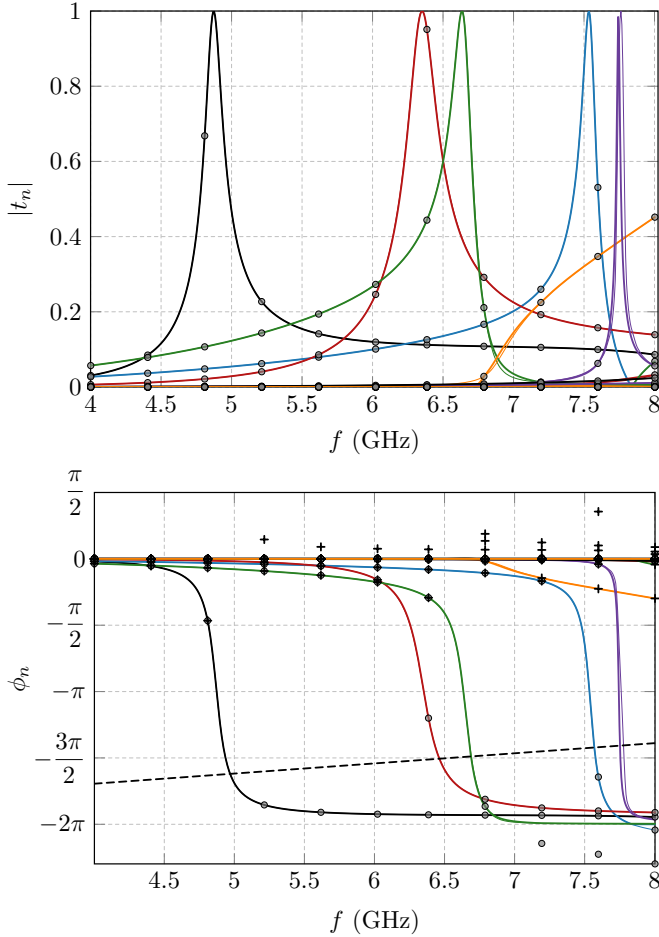


Fig. 5. Modal significance $|t_n|$ (top) and phase ϕ_n (bottom) for a dielectric cylinder with height 4.6 mm, radius 5.25 mm, and relative permittivity $\epsilon_r = 38$ calculated using (34) with a PMCHWT formulation. Thick lines show interpolation based on rational functions (43) together with (45) using 11 sample points which are indicated with markers. Thin lines are based on 100 sample points and phase unwrapping (48). Intersection between the phase ϕ_n and the dashed line approximates the poles ξ_m of the rational function (43).

B. Dielectric Cylinder

The benchmark example from [49], [50], [75] consisting of a cylindrical dielectric resonator with height 4.6 mm, radius 5.25 mm, and relative permittivity $\epsilon_r = 38$ is used to illustrate the potential of the proposed methodology on a challenging and well-studied case. The PMCHWT formulation is used to obtain the impedance matrix. The modal significance $|t_n|$ and phase ϕ_n evaluated from (15) and (23) are depicted in Fig. 5 showing five distinct peaks corresponding to TE_{01} , HEM_{11} , HEM_{12} , TM_{01} , and HEM_{21} modes, in agreement with the results in [49], [75]. The corresponding surface currents calculated from (35) at the resonance frequencies are depicted in Fig. 6.

The results in Fig. 5 also illustrate interpolation using rational functions (43) together with (45). The rational fit uses 11 equidistant frequency points, shown with black markers, to compute the poles and residues in Table II of the dominant diagonal elements T_{nn} corresponding to the peaks in Fig. 5. This diagonal matrix is used to construct a scattering matrix

TABLE II
COEFFICIENTS IN UNIT m^{-1} OF THE RATIONAL FIT (43) OF THE DIAGONAL ELEMENTS T_{nn} USED TOGETHER WITH $b_0 = 1/r_\Omega \approx 174 m^{-1}$ TO CALCULATE THE CURVES IN FIG. 5.

	TE_{01}	HEM_{11}	HEM_{12}	TM_{01}	HEM_{21}
ξ_1	104	135	140	159	162
b_1	4.59	4.85	1.78	1.29	0.363
ξ_2	199		247		
b_2	5.44		51.2		
b_∞	1242	667	380	299	518

S_1 containing dominant contributions of the resonances. These resonances are removed from S using (46) to synthesize a scattering matrix S_2 with slower frequency variation which is interpolated using (45). The resulting curves for modal significance $|t_n|$ and angle ϕ_n tracked using (47) are shown in Fig. 5 by solid curves with colors distinguishing different modes. Intersections between the dashed line, illustrating the resonance condition $\phi_n + 2kr_\Omega = -\pi$ for the phase shifted scattering matrix (41), and curves are related to the resonance frequencies in the rational model (43) as given in Table II. The interpolation results are compared with results based on 100 sample points tracked using (47) and plotted with thin solid lines. This dense sampling was used to resolve narrowband resonances. The thin lines are mostly indistinguishable from the thicker lines, *i.e.*, the curves coincide, which validates the rational approximation (42) combined with (45) using (46). The rational fit (43) finds all peaks, although they are not sampled in the original computation (11 sample points) and only a slight shift (compared with the thin lines) is seen for the HEM_{21} mode. The interpolation (46) based on this small number of sampling points causes some errors, *e.g.*, the minor disturbances around 6.7 GHz.

Interpolation based on phase unwrapping (48) of tracked modes (47) is also illustrated in the bottom panel of Fig. 5. Sampling at only 11 points misses most peaks and the resulting phase ϕ_n is close to zero for most of the sampled points as shown by the + markers in Fig. 5. Modal tracking (47) based on these 11 sample points and ordinary phase unwrapping does not affect the phase. Nevertheless, making the eigenvalues s_n lossless by the phase shift $\exp(-2jkr_\Omega)$, *cf.* (41), and invoking Foster's theorem in the phase unwrapping (48) decreases many sample points $\phi_n(k_q)$ by a factor -2π as shown by the corresponding circular markers. This unwrapped phase can be interpolated with standard low or high order algorithms and produces curves crossing the line $\phi_n = -\pi$ at scattering (external) resonances with $t_n = -1$. One notable error in unwrapping of the tracked modes is observed for the HEM_{12} mode, where the tracking (based on 11 samples) misses the onset of a new mode around 6.7 GHz and predicts a phase following the circular markers below $\phi_n = -2\pi$.

The estimate (61) with $\iota = 7$ is conservative and in many practical applications it is sufficient to compute only a few of the lowest-order characteristic modes, *i.e.*, those with smallest eigenvalue magnitude $|\lambda_n|$. The examples previously presented in this paper were computed with $\iota = 7$ and $\iota = 2$ and the differences were negligible for modes with modal significance $|t_n| > 0.01$. Using $\iota = 2$ reduces the degree of the spherical

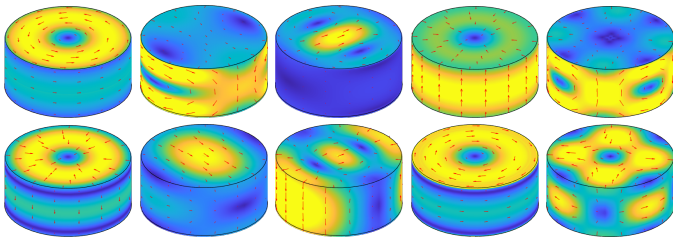


Fig. 6. Characteristic current densities \mathbf{J}_n (top) and \mathbf{M}_n (bottom) for the resonance frequencies of the dielectric cylinder in Fig. 5 computed from the eigenvectors \mathbf{f}_n using (35). From left to right, the depicted currents correspond to modes: TE_{01} at 4.87 GHz, HEM_{11} at 6.35 GHz, HEM_{12} at 6.63 GHz, TM_{01} at 7.53 GHz, and HEM_{21} at 7.76 GHz.

waves to $L_{\max} = 12$, *i.e.*, to 336 spherical waves in total. In this configuration, the computational cost is dominated by the calculation of $\mathbf{Z}^{-1}\mathbf{U}^T$ in (34). The computation of all characteristic numbers, characteristic modes, and their tracking is computationally much less expensive.

C. PEC Plate

A square PEC plate is used to illustrate the capabilities of the tracking and higher-order interpolation of the unwrapped phase described in Section VI. The impedance matrix is computed in 14 sample points equidistantly placed in the interval $kr_{\Omega} \in [0.1, 10]$ using EFIE with 7080 basis functions. Parameters $kr_{\Omega} = 10$ and $\nu = 2$ were used in (61) giving $L_{\max} = 18$ and 720 spherical waves. The phases ϕ_n of modes tracked via (47) are unwrapped, interpolated using Akima interpolation [76], and plotted in Fig. 7. The phase values resulting from the eigenvalue decomposition (22) are highlighted by markers. For ease of presentation, the unwrapped modal phases $\{\phi_n\}$ are plotted outside the usual interval $(-\pi, \pi)$. It is nevertheless important to realize that the phase ϕ_n is ambiguous by addition of multiples of 2π and that different phase plots might correspond to the same physical scenario unambiguously characterized by the complex number s_n or t_n . Extreme cases of $\phi_n = \pm\pi$ are physically the same and correspond to external resonance ($\lambda_n = 0$).

Evaluation of the results in Fig. 7 from precomputed matrices \mathbf{Z} and \mathbf{U} took 60 s (using MATLAB and i7-9700k CPU @ 3.6GHz with 64 GB RAM) and was dominated by 59 s used for evaluation of matrix \mathbf{T} via relation (34) in the 14 sample points. In contrast, only 1 s was required for eigenvalue decomposition of the matrix \mathbf{T} , tracking, and interpolation. The same time of 60 s would be needed for the evaluation of only 10 dominant characteristic modes using the generalized eigenvalue decomposition (36) in the 14 sample points using $\text{eigs}(\mathbf{X}, \mathbf{R})$ function in MATLAB. Reducing the discretization to 3120 basis functions reduces the aforementioned evaluation time to 6 s using matrix \mathbf{T} and to 8 s using the decomposition (36). These results indicate that the evaluation of the matrix \mathbf{T} using (34) has a computational cost similar to the cost of evaluating a few dominant characteristic modes using (36). The additional computational cost of eigenvalue decomposition (15), correlation tracking (47), and interpolation is negligible, making the scattering-based approach superior

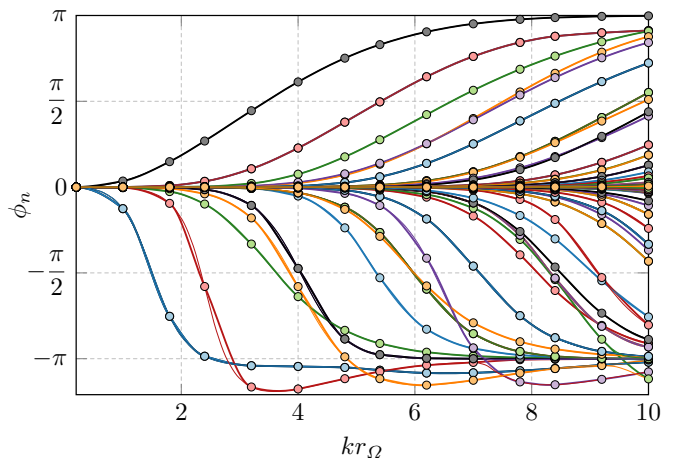


Fig. 7. Phase ϕ_n for a square PEC plate computed from 14 equidistant sample points (markers) using correlation tracking (47) and higher order interpolation of the unwrapped phase (48) (thick lines). The data are compared with the corresponding case using 50 sample points (thin lines).

in cases when characteristic numbers are to be calculated over broad frequency ranges.

D. Lossy Dipoles

Two thin and closely spaced dipoles are used to illustrate tracking of characteristic modes for structures with resonances and symmetries, as well as to show effects of losses. Consider two strip dipoles with lengths ℓ and ℓ_1 , strip widths 0.01ℓ , separated by a distance 0.2ℓ , and modeled by a surface resistivity $R_s \in \{0, 10^{-2}, 10^{-1}\} \Omega/\square$ as depicted in the inset of Fig. 8.

Lossless structures ($R_s = 0$, solid curves in Figs. 8 and 9) are used first to examine the ability of correlation tracking (47) to properly identify eigenvalue crossings and crossing avoidances. Magnitudes $|t_n|$ (the modal significance) for the cases of two dipoles with the same length $\ell = \ell_1$ and dissimilar lengths $\ell_1 = 0.99\ell$ are depicted in the top and bottom panels of Fig. 8, respectively. The corresponding phase angles α_n (phase of eigenvalue t_n) are shown in Fig. 9. Two characteristic modes (even and odd modes) dominate around the first resonance $\ell \approx 0.5\lambda$ as illustrated by black and red solid curves. Higher-order modes have very low modal significance $|t_n| \approx 0$ and ill-defined phase α_n and are not shown in the figures. The frequency interval $l/\lambda \in [0.44, 0.52]$ is sampled with 200 sample points and the result of tracking (47) shows that eigentraces cross (in phase and in magnitude) for $\ell_1 = \ell$ but do not cross (in phase) for $\ell_1 = 0.99\ell$ in agreement with the von Neumann-Wigner theorem [33], [61], [77]. The differences between eigenvalues and eigenvectors for the two cases are negligible away from the resonance at $l/\lambda \approx 0.48$ and the tracking algorithm requires sample points close to the resonance to distinguish the two cases.

Dipoles with non-zero surface resistivity are used to illustrate properties of characteristic modes for lossy structures. Lossless and low-loss cases are indistinguishable in the phase α_n , as seen in Fig. 9, but a small amplitude decrease is visible in modal significance $|t_n|$. The differences increase

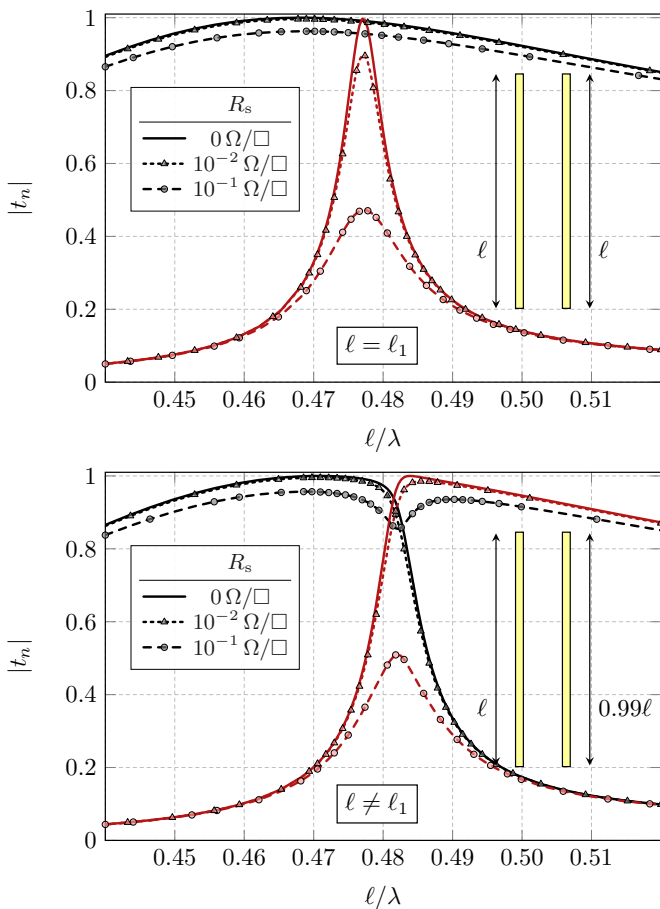


Fig. 8. Modal significance for two dipoles with lengths ℓ and ℓ_1 , with $\ell/100$, separated by a distance $\ell/5$ (outside to outside) and modeled with surface resistivity $R_s \in \{0, 10^{-2}, 10^{-1}\} \Omega/\square$ as indicated by the legend. Two dominant modes (even and odd modes) are shown by black and red curves. Top figure corresponds to identical dipoles $\ell = \ell_1$ while the bottom figure corresponds to lengths $\ell_1 = 0.99\ell$.

with higher losses and the case with $R_s = 0.1 \Omega/\square$ is clearly noticeable. Here, the eigentraces (both in phase and magnitude) of equal-lengths and different-lengths cases are similar (dashed curves), both presenting crossing-avoidances dominated by very different values of modal significance of the even and odd mode at the resonance frequency. By means of (56), this can be attributed to different modal radiation efficiencies $\eta_n = (1 + \delta_n)^{-1} = -|t_n|/\cos(\alpha_n)$ of the even and odd modes, since at the external resonance $\cos(\alpha_n) = -1$ the modal radiation efficiency equals the modal significance.

Losses also affect orthogonality of the far fields, here represented by the eigenvectors \mathbf{f}_n . In reciprocal scenarios, the modal eigenvectors always satisfy relation (53), *i.e.*, modes belonging to different eigenvalues exhibit vanishing reaction product, see the top row of in Fig. 10. In the general lossy scenario, the modes are however not orthogonal as can be seen from the bottom row of Fig. 10 which depicts correlation coefficients ρ_{mn} given by (54). The reaction product is diagonal for all considered cases. The matrix of correlation coefficients, however, is diagonal for the lossless case whereas the lossy cases have non-negligible correlation between the two dominant modes. This correlation ρ_{12} is detailed in Fig. 11 around

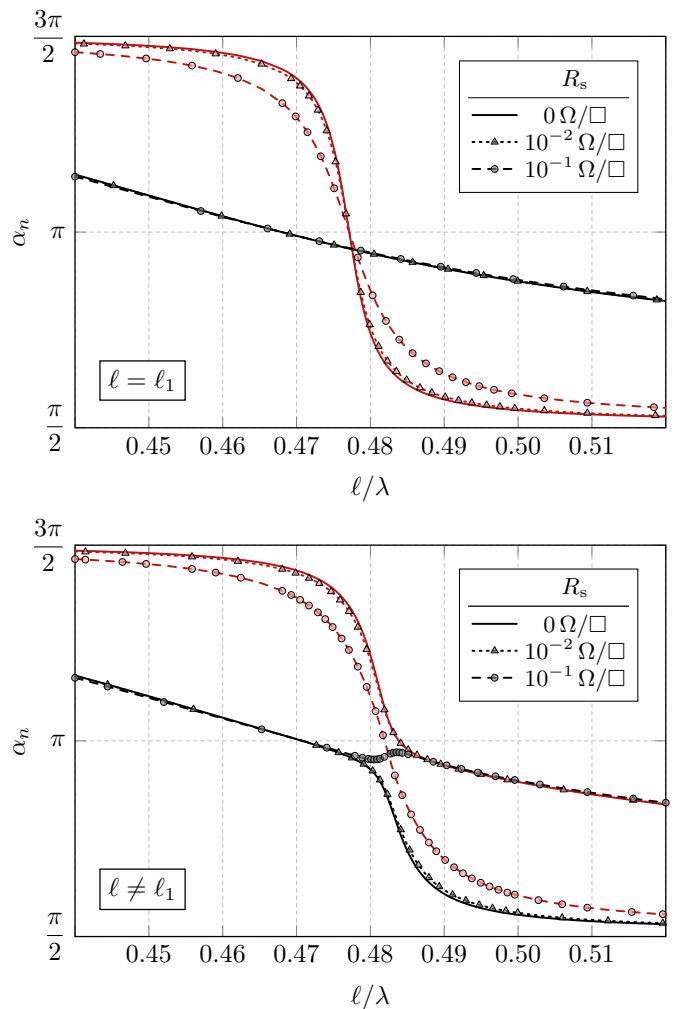


Fig. 9. Phase α_n for a setup identical with Fig. 8

the resonance frequency, where it is seen that the correlation is $|\rho_{12}| \approx 0.3$ at $\ell = 0.48\lambda$ for $R_s \in \{0.01, 0.1\} \Omega/\square$ but vanishes quickly away from the resonance. The correlation matrix for the $\ell_1 = \ell$ case is approximately diagonal around the resonance but has non-diagonal elements for higher order modes at higher frequencies. In that case, the orthogonality, *i.e.*, $\rho_{12} = 0$, follows from the symmetry of the structure which divides the dominant modes into different irreducible representations [72].

IX. DISCUSSION

This section discusses several important points raised throughout this paper, with emphasis placed on their interpretation within the context of contemporary characteristic mode theory.

A. Uniqueness of Characteristic Mode Decomposition

The set of characteristic modes for a given scatterer should be unique and independent of the numerical method used to obtain them. This assumption is fulfilled with the scattering formulation (15) and the link between an impedance and the

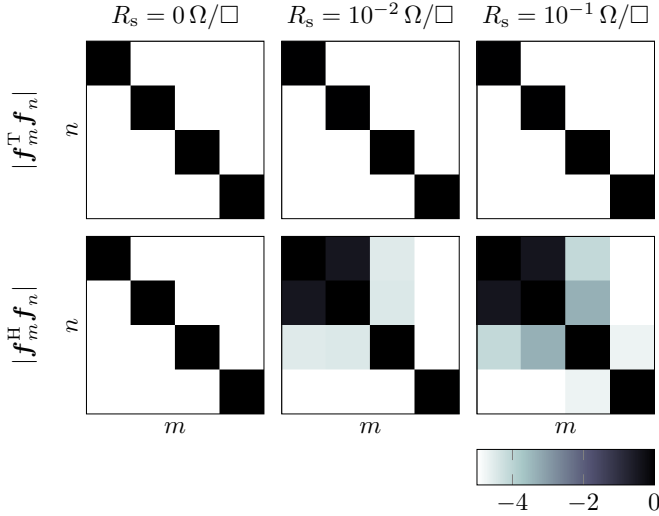


Fig. 10. The reaction products $|\mathbf{f}_m^T \mathbf{f}_n|$ (top) and correlation coefficients $|\rho_{mn}| = |\mathbf{f}_m^H \mathbf{f}_n|$ (bottom) for the first four characteristic modes at resonant frequency of the dipoles with lengths $\ell_1 = 0.99\ell$.

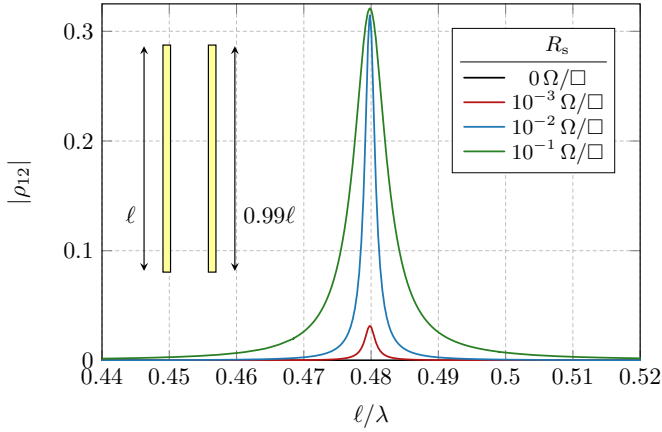


Fig. 11. Correlation coefficient between the two dominant characteristic modes of two dipoles with length ℓ and 0.99ℓ and different values of surface resistivity.

scattering formulation (34), which is valid for all method-of-moments formulations. Other numerical methods may also be used, *e.g.*, finite element method [37], [38], finite difference frequency-domain method [39], or null-field method [35]; so long as a transition matrix \mathbf{T} can be constructed. This indicates that characteristic mode analysis does not require the use of the MoM [78].

Another advantage of the scattering formulation is its lack of spurious modes. Once the transition matrix \mathbf{T} is calculated, its decomposition is immune to the presence of internal resonances ($t_n = 0$). However, it should be noted that its construction via (34) is difficult in this case due to potential singularities of the impedance matrix \mathbf{Z} .

B. Numerical Dynamics and Computational Cost

Using fixed numerical precision, the scattering- and impedance-based approaches perform similarly in terms of computational time for electrically small problems. For electrically larger problems, the scattering approach is faster than

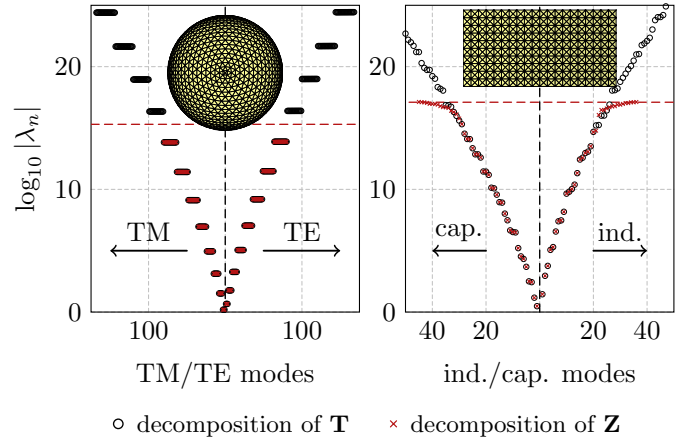


Fig. 12. Characteristic modes evaluated with scattering and impedance formulation, (15) and (36), respectively. A spherical shell discretized into 2400 triangles (3600 RWG basis functions) and a rectangular plate of aspect ratio 2 : 1 discretized into 800 triangles (1170 RWG basis functions) are studied. Both obstacles are made of PEC and of electrical size $kr_\Omega = 1$. The decomposition is evaluated with generalized Schur decomposition. The characteristic numbers of the spherical shell exceeding dashed line were evaluated as infinite by the used routine and are therefore not shown.

a MoM implementation of the impedance formulation. With respect to electrical size, the impedance matrix \mathbf{Z} scales quadratically for surface formulations and cubically for volume formulations, whereas the transition matrix \mathbf{T} scales quadratically in both cases. Furthermore, the number of spherical waves is typically orders of magnitude smaller than the number of local basis functions. Hence, the transition matrix method is expected to generally require less computational time as it is its construction, not its eigenvalue decomposition, which accounts for the majority of the overall computational cost.

Figure 12 compares magnitudes of characteristic numbers produced by both decomposition methods applied to a spherical shell and a rectangular plate. In the case of the spherical shell, 3600 RWG basis functions and 510 spherical waves ($L_{\max} = 15$) are used in the impedance- and scattering-based methods, respectively. Despite involving significantly more unknowns, the impedance method has numerical dynamics saturated at double precision (red dashed line), while the scattering formulation might offer higher dynamics. In the case of the irregular (in the context of spherical symmetry) rectangular plate, 1170 RWG and 510 spherical waves are used. Here the relative size, and thus computational cost, of the two solutions are comparable, however the scattering-based method still affords improved numerical dynamics beyond those of the impedance-based solution.

Beyond computational cost and numerical dynamics, a notable advantage of scattering method over impedance method is applicability of a tracking procedure described in Section VI, based on rational fit and interpolation of scattering matrix. This is supported by a case study given in Section VIII-C, where the computational times were recorded for decomposition of a PEC plate.

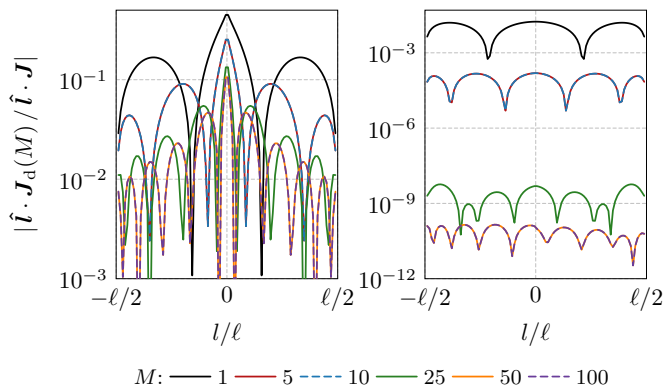


Fig. 13. Relative error of the sum (62) of characteristic modes evaluated via (15) and (35). A thin-strip PEC dipole oriented along direction $\hat{\mathbf{l}}$, discretized into 400 triangles (499 RWG basis functions), and having electrical size $kr_\Omega = 2\pi/3$ is studied. The excitation used is a delta gap feeder placed in the middle of the dipole (left) and a plane wave incident perpendicularly to the plane of the dipole and with polarization along the dipole.

C. Convergence of Characteristic Mode Superposition

Characteristic modes are known to be problematic [8], [9] in describing certain scenarios, such as those in which the incident field (described by the vector \mathbf{V}) is produced by localized sources within Ω . This issue is illustrated in Fig. 13 using a thin-strip PEC dipole excited by a delta gap source (source within the convex hull of region Ω) or a plane wave (far-field source). In both cases, the residual [9] current $\mathbf{I}_d(M) = \mathbf{I} - \mathbf{I}(M)$ is evaluated, where the vector $\mathbf{I} = \mathbf{Z}^{-1}\mathbf{V}$ comes from a direct solution of the scattering problem, while vector $\mathbf{I}(M)$ is evaluated using a summation formula⁹ [2]

$$\mathbf{I}(M) = \sum_{n=1}^M \frac{1}{(1 + j\lambda_n)} \frac{\mathbf{I}_n^T \mathbf{V}}{\mathbf{f}_n^T \mathbf{f}_n} \mathbf{I}_n = - \sum_{n=1}^M t_n \frac{\mathbf{I}_n^T \mathbf{V}}{\mathbf{f}_n^T \mathbf{f}_n} \mathbf{I}_n. \quad (62)$$

It is observed in Fig. 13 that decomposition of the current (62) excited by a delta-gap source fails to converge.

The scattering-based description of characteristic modes shown in this paper offers an explanation to this phenomenon. The connection between transition and impedance matrix based characteristic modes is provided via relation (31). This relation is, nevertheless, only valid for sources which produce incident fields of the form of (9), *i.e.*, if a sphere centered at origin exists that separates sources of incident field from the scatterer. Since the scatterer might be arbitrarily shifted with respect to origin, relation (31) allows for the modeling of sources anywhere outside the convex hull of region Ω , see Fig. 1. No such shift, however, allows for a separating sphere to be drawn for sources inside this convex hull (such as delta gap source). It should also be realized that as the source of the incident field approaches the convex hull, the radius of the corresponding separating sphere differs greatly

⁹Notice that the formula assumes a symmetric transition matrix (reciprocity) and that matrix transposition inside the formula can be interchanged with Hermitian conjugation in lossless scenarios where eigenvectors $\mathbf{f}_n, \mathbf{I}_n$ can be chosen real-valued, see Section III. Unlike in [2] we have also chosen to write the term $\mathbf{f}_n^T \mathbf{f}_n$ in the denominator instead of usual term $\mathbf{I}_n^T \mathbf{R}_0 \mathbf{I}_n$ which is only valid in specific formulations of field integral equations.

from that of the smallest sphere circumscribing the scatterer and it is the radius of the former that should be used in (61) to describe such scenario, making the summation formula (62) impractical or even insufficient when the finite precision of numerical characteristic modes decompositions is considered.

The aforementioned issues can also be viewed from a different perspective. Imagine that the true current \mathbf{I} induced on a scatterer is known and with it the expansion vector \mathbf{f} , see (33), representing the electric far field. Employing relation (35) it can be seen that the summation formula (62) can be rewritten as

$$\mathbf{I}(M) = \sum_{n=1}^M \frac{\mathbf{f}_n^T \mathbf{f}}{\mathbf{f}_n^T \mathbf{f}_n} \mathbf{I}_n, \quad (63)$$

where it is observed that the summation coefficients are projections of the total electric far field into modal far fields, *i.e.*, a quantity that is insensitive to any near-field distributions. Characteristic modes are therefore not well suited to expand current densities on scatterers excited by sources located in the near field of the region Ω .

Despite these difficulties, characteristic modes are appropriate to expand scattering properties, such as radiated far fields described by the vector \mathbf{f} . To that point, a formula analogous to (62) can be written as

$$\mathbf{f}(M) = \sum_{n=1}^M t_n \frac{\mathbf{f}_n^T \mathbf{a}}{\mathbf{f}_n^T \mathbf{f}_n} \mathbf{f}_n, \quad (64)$$

the convergence of which, unlike of (62), is favorable, especially in the case of electrically small scatterers.

D. Spherical Waves as Extended Ports

An interesting point of view on the connection between transition and impedance matrices (34) is obtained through examination of a network representation [79] and port modes [34]. The port admittance matrix \mathbf{y} of a multiport antenna is expressed as

$$\mathbf{y} = \mathbf{P}^T \mathbf{Z}^{-1} \mathbf{P} = \mathbf{P}^T \mathbf{Y} \mathbf{P}, \quad (65)$$

where the columns of the matrix \mathbf{P} define ports [79], *i.e.*, the excitation vector \mathbf{V} is given as

$$\mathbf{V} = \mathbf{P} \mathbf{v}, \quad (66)$$

where \mathbf{v} is a column vector of port voltages. Relation (65) resembles (34) provided that matrix \mathbf{T} is associated with normalized port admittance matrix \mathbf{y} and matrix \mathbf{P} is associated with normalized matrix \mathbf{U} . In this way, the spherical waves act as ports which can be incorporated into a complete port characterization of the antenna similar to the antenna scattering matrix [10], [43]

$$\begin{bmatrix} \mathbf{P}^T \mathbf{Y} \mathbf{P} & \mathbf{P}^T \mathbf{Y} \mathbf{U}^T \\ \mathbf{U} \mathbf{Y} \mathbf{P} & \mathbf{U} \mathbf{Y} \mathbf{U}^T \end{bmatrix} \begin{bmatrix} \mathbf{v} \\ \mathbf{a} \end{bmatrix} = \begin{bmatrix} \mathbf{i} \\ -\mathbf{f} \end{bmatrix}. \quad (67)$$

The network characteristic modes [80]

$$\mathbf{y} \mathbf{v}_n = (1 - j\lambda_n) \text{Re} \{ \mathbf{y} \} \mathbf{v}_n \quad (68)$$

then directly translate to

$$\mathbf{T} \mathbf{f}_n = (1 - j\lambda_n) \text{Re} \{ \mathbf{T} \} \mathbf{f}_n, \quad (69)$$

which, combining (15) and (71), holds for loss-less scatterers.

E. Substructure Modes in the Scattering Formulation

Substructure modes introduced in [81] have a potential to reduce the size of a problem and offer a good alternative to the network (port-mode) representation discussed in Section IX-D. Their evaluation is based on Schur complement [47] which assumes an excitation field on the uncontrollable part of the structure which is solely due to currents on the controllable region.

This assumption is, however, not met with the scattering approach (15), since it was shown in (65) that the scattering formulation is formally similar to a port-mode representation. Such a description is in general incompatible with division into substructures.

The scattering formulation is, therefore, not compatible with the substructure modes as defined in [81], however, there might be an alternative approach devised in the future, which will preserve the essential properties of substructure modes (mainly the possibility to compress the size of the problem).

F. Modes for Lossy Objects

There is no consensus in the literature on how to define characteristic modes for lossy objects, and it is not possible to preserve all the good properties from the lossless case. As shown in Section VII diagonalization of matrix \mathbf{T} (or similarly matrix \mathbf{Z}) is in general not possible with modes having orthogonal far fields. However, numerical results in Section VIII-D indicate that ohmic losses commonly used to model metallic antennas only slightly perturb the modes and produce modes with low correlation (54), see also [6], [82]. Moreover, the characteristic mode superposition (62) only requires diagonal reaction products (53), which holds for lossy materials [2].

Alternative possibilities to diagonalize matrices include the Autonne–Takagi factorization, which for reciprocal \mathbf{T} is $\mathbf{A}^T \mathbf{T} \mathbf{A} = \mathbf{\Lambda}$ with a unitary matrix \mathbf{A} and a diagonal matrix $\mathbf{\Lambda}$ having the singular values of \mathbf{T} on the diagonal. This constructs modes with orthogonal far fields but without many of the good properties from ordinary diagonalization [47], such that summation (62). Autonne–Takagi factorization is similar to diagonalization of $\mathbf{T}^H \mathbf{T}$ as proposed in [83] and discussed for lossy cases in [78]. Similar properties are also obtained from diagonalization of $\text{Re}\{\mathbf{T}\}$.

Generalizations directly based on the impedance matrix have also been investigated. In [2], it is shown that using the resistive part of the impedance matrix as a weighting matrix lead to modes with correlated far fields and modes with a combination of high losses and radiation. Radiation modes [84], [85] is an alternative which produces modes with orthogonal far fields but independent of the reactance.

X. CONCLUSION

The focus of this work is the connection between scattering- and impedance-based formulations of characteristic modes. While the impedance-based formulation is now the standard in the literature, it suffers from several issues; not the least of which is its ambiguous generalization to lossy systems. As demonstrated in this work, the scattering-based approach

alleviates many of these issues and clarifies why characteristic modes (as they were originally formulated) lose far-field orthogonality on lossy structures.

The scattering-based approach studied in this work requires the computation of the transition matrix, a structure not typically available from MoM numerical tools. However, computation of the transition matrix within a MoM routine involves minimal computational overhead and only requires the calculation of basis function projections onto spherical harmonics. Also, the use of the transition matrix, as opposed to a MoM impedance matrix, generalizes the calculation of characteristic modes to any computational method capable of producing a transition matrix, including finite difference time domain and finite element methods. This lack of dependence on a chosen numerical method implies the consistent definition of characteristic modes for problems involving any lossless materials with no change to the underlying eigenvalue problem, greatly expanding the applicability of characteristic modes beyond MoM formulations.

The examples in this work demonstrate several computational advantages arising from the use of scattering-based characteristic mode formulations. In some cases, significant improvements in numerical dynamics and computational cost are observed for single-frequency calculations. Additionally, the interpolation and tracking methods enabled by the properties of the transition matrix allows for a sizeable reduction in the number of single-frequency calculations required to synthesize accurate broadband characteristic mode data.

A few open problems remain in the use of scattering-based characteristic mode formulations. Namely, the ability of characteristic modes to represent the behavior of systems excited by localized, near-field sources (*e.g.*, discrete antenna ports) remains to be rigorously determined. Additionally, the issue of applying characteristic mode analysis to represent the behavior of disjoint or non-convex scatterers is elucidated by the scattering-based formulation. The study of these fundamental questions from scattering-based perspectives will continue to steer the understanding and use of characteristic modes, regardless of the specific numerical tool or formulation adopted by individual practitioners.

APPENDIX A

NORMALITY OF TRANSITION MATRICES AND UNITARITY OF SCATTERING MATRICES

Using expansion (1) and (9), the net power exiting a surface S fully enclosing the scatter Ω can be evaluated as [12]

$$P_S = \frac{1}{2} \text{Re} \oint_S (\mathbf{E} \times \mathbf{H}^*) \cdot d\mathbf{S} = \frac{1}{2} \left(|\mathbf{f}|^2 + \text{Re}\{\mathbf{a}^H \mathbf{f}\} \right), \quad (70)$$

where the first term on the right-hand side represents the outward power flux, *i.e.*, the scattered power in (12), while the second term is minus the cycle mean power supplied by sources external to the scatterer.

For a lossless scatterer the net power P_S must vanish for any incident field described by vector \mathbf{a} . Substituting from (10) there must be

$$\mathbf{T}^H \mathbf{T} = -\text{Re}\{\mathbf{T}\}, \quad (71)$$

where the real and imaginary part of a matrix are understood as

$$\begin{aligned}\operatorname{Re}\{\mathbf{T}\} &= \frac{1}{2}(\mathbf{T} + \mathbf{T}^{\text{H}}), \\ \operatorname{Im}\{\mathbf{T}\} &= \frac{1}{2j}(\mathbf{T} - \mathbf{T}^{\text{H}}).\end{aligned}\quad (72)$$

Relation (71) leads to the following vanishing commutators

$$\left[\operatorname{Re}\{\mathbf{T}\}, \operatorname{Im}\{\mathbf{T}\}\right] = \mathbf{0} \quad \text{and} \quad \left[\mathbf{T}, \mathbf{T}^{\text{H}}\right] = \mathbf{0} \quad (73)$$

proving that the transition matrix \mathbf{T} of a lossless scatterer is a normal matrix. The spectral theorem [47, Chap. 2.5] states that a matrix is unitarily diagonalizable if and only if the matrix is normal, providing an unambiguous requirement for orthogonal eigenvectors.

Relation (71) together with relation (11) directly leads to

$$\mathbf{S}^{\text{H}}\mathbf{S} - \mathbf{1} = \mathbf{0} \quad (74)$$

showing that the scattering matrix \mathbf{S} of a lossless scatterer is unitary [45, Chap. 4]. Lorentz reciprocity further implies [45, Chap. 4] that objects made of reciprocal materials have symmetric scattering matrices $\mathbf{S} = \mathbf{S}^{\text{T}}$ as well as transition matrices $\mathbf{T} = \mathbf{T}^{\text{T}}$.

The unitarity of lossless, reciprocal scattering matrices implies unitary eigenvalues $|s_n| = 1$. Complex conjugation of the underlying eigenvalue problem (22), multiplication with \mathbf{S}_{s_n} , and use of the symmetric nature of the scattering matrix gives

$$\mathbf{S}\mathbf{f}_n^* = s_n \mathbf{f}_n^*, \quad (75)$$

showing that \mathbf{f}_n and \mathbf{f}_n^* are both eigenvectors of \mathbf{S} . Hence, the phase of the eigenvector \mathbf{f}_n is arbitrary such that it may be chosen to be real valued.

In lossy systems, the normality of matrix \mathbf{T} and unitarity of matrix \mathbf{S} is generally lost which can be linked to time-reversal symmetry [86, Chap. 6]. Assuming reciprocity $\mathbf{T}^{\text{T}} = \mathbf{T}$ and using the fact that \mathbf{T} is normal if and only if [87]

$$\|\mathbf{T}\mathbf{a}\| = \|\mathbf{T}^*\mathbf{a}\| \quad (76)$$

for all \mathbf{a} , it is observed that the lack of time-reversal symmetry, $\mathbf{T} \neq \mathbf{T}^*$, leads to the loss of normality unless special circumstances, such as a diagonal matrix \mathbf{T} , occur.

APPENDIX B

DIFFERENT SCHEMES FOR CONVERSION OF MATRIX \mathbf{Z} INTO MATRIX \mathbf{T} .

This appendix shows several of the most frequent forms of field integral equations, their method-of-moments formulations, and explicit forms of relations between the associated impedance and transition matrices. The formulation for penetrable bodies based on surface equivalence principle [27] is not shown as it is detailed in Section IV.

A. \mathbf{J}^e – EFIE

The electric field integral equation (EFIE) is the most common formulation of scattering from dielectric or highly electrically conductive obstacles. Employing the notation introduced in Section II, the integral equation reads

$$\rho \mathbf{J}^e + jZk\mathcal{L}\{\mathbf{J}^e\} = \mathbf{E}^i. \quad (77)$$

In the case of volumetric formulation for dielectric obstacles, equality (77) is enforced throughout the obstacle, which is assumed to be described by the (possibly inhomogeneous) complex resistivity

$$\rho = -j\frac{Z}{k}\chi^{-1} \quad (78)$$

with χ being electric susceptibility. In the case of highly conducting obstacle, the equality (77) is enforced only at the surface of the obstacle and the term $\rho \mathbf{J}^e$ is substituted by $Z_s \mathbf{J}^e$ with Z_s representing a surface impedance [86], [88] and with \mathbf{J}^e being a surface current density.

A method-of-moments formulation in this case reads

$$\mathbf{Z}^{ee}\mathbf{I}^e = \mathbf{V}^e \quad (79)$$

and the transition matrix \mathbf{T} can be evaluated as

$$\mathbf{T} = -\mathbf{U}_1 (\mathbf{Z}^{ee})^{-1} \mathbf{U}_1^{\text{T}} \quad (80)$$

and the radiation operator \mathbf{R}_0 reads

$$\mathbf{R}_0 = \mathbf{U}_1^{\text{H}}\mathbf{U}_1 \quad (81)$$

and conversion from spherical expansion coefficients to current expansion coefficients of characteristic modes reads

$$\mathbf{I}_n^e = t_n^{-1} (\mathbf{Z}^{ee})^{-1} \mathbf{U}_1^{\text{H}}\mathbf{f}_n. \quad (82)$$

The generalized eigenvalue problem for characteristic modes based on matrix \mathbf{Z}^{ee} in this case leads to well-known relation [2]

$$\mathbf{Z}^{ee}\mathbf{I}_n^e = (1 + j\lambda_n) \mathbf{R}_0\mathbf{I}_n^e, \quad (83)$$

where in loss-less cases $\operatorname{Re}\{\mathbf{Z}^{ee}\} = \mathbf{R}_0$.

B. \mathbf{J}^e – MFIE

Another common formulation of scattering from closed perfectly electrically conducting objects is the magnetic field integral equation (MFIE), which reads

$$-\frac{1}{2}\hat{\mathbf{n}} \times \mathbf{J}^e - \mathcal{K}\{\mathbf{J}^e\} = \mathbf{H}^i. \quad (84)$$

The equation is imposed over the closed conducting surface Ω with outward-directed normal $\hat{\mathbf{n}}$. Using the notation from Section IV, the method-of-moments formulation in this case reads

$$\mathbf{Z}^{\text{me}}\mathbf{I}^e = \mathbf{V}^{\text{m}} \quad (85)$$

and the $\mathbf{Z} \rightarrow \mathbf{T}$ conversion formula reads

$$\mathbf{T} = \mathbf{U}_1 (j\mathbf{Z}^{\text{me}})^{-1} \overline{\mathbf{U}}_1^{\text{T}}. \quad (86)$$

Characteristic currents are in this case evaluated as

$$\mathbf{I}_n^e = -t_n^{-1} (j\mathbf{Z}^{\text{me}})^{-1} \overline{\mathbf{U}}_1^{\text{T}}\mathbf{f}_n, \quad (87)$$

which can also be transformed into a generalized eigenvalue problem

$$-j\mathbf{Z}^{\text{me}}\mathbf{I}_n^e = (1 + j\lambda_n)\bar{\mathbf{U}}_1^T\mathbf{U}_1\mathbf{I}_n^e, \quad (88)$$

which has a form proposed in [89] assuming $\text{Im}\{\mathbf{Z}^{\text{me}}\} = \bar{\mathbf{U}}_1^T\mathbf{U}_1$, which holds for lossless scatterers.

Problem (88) resembles (83) but there are notable differences. The radiation operator \mathbf{R}_0 is still given by (81) and is not equal to the matrix appearing on the right-hand side of (88). This invalidates the diagonalization of the system matrix \mathbf{Z}^{me} with the eigencurrents \mathbf{I}_n^e . Instead, and similarly to the left and right eigenvectors in [6], a dual current

$$\bar{\mathbf{I}}_n^e = -t_n^{-1}(j\mathbf{Z}^{\text{me}})^{-T}\mathbf{U}_1^T\mathbf{f}_n, \quad (89)$$

is introduced by exchanging TM spherical waves and TE spherical waves which is motivated by the off diagonal position of matrix \mathbf{Z}^{me} in the impedance matrix (28). Using that the matrix \mathbf{T} is symmetric (reciprocity), it can be seen that

$$\mathbf{f}_n = -\bar{\mathbf{U}}_1\bar{\mathbf{I}}_n^e \quad (90)$$

and hence

$$\begin{aligned} -(\bar{\mathbf{I}}_m^e)^H j\mathbf{Z}^{\text{me}}\mathbf{I}_n^e &= (1 + j\lambda_n)(\bar{\mathbf{I}}_m^e)^H \bar{\mathbf{U}}_1^T\mathbf{U}_1\mathbf{I}_n^e \\ &= (1 + j\lambda_n)\mathbf{f}_m^H\mathbf{f}_n = (1 + j\lambda_n)\delta_{mn} \end{aligned} \quad (91)$$

which is consistent with (40) if the magnetic current is identified with the dual current.

C. J^e – CFIE

In order to avoid internal resonance problems [19], [90], a linear combination of the EFIE (77) and MFIE (85) formulations

$$\alpha\text{EFIE} + Z(1 - \alpha)\hat{\mathbf{n}} \times \text{MFIE} \quad (92)$$

with $\alpha \in (0, 1)$ is commonly imposed over the surface of a closed perfectly conducting obstacle to solve the corresponding scattering scenario. The resulting equation is called the combined field integral equation (CFIE). The CFIE involves only electric currents represented by \mathbf{I}^e ,

$$\mathbf{Z}^{\text{ee}}\mathbf{I}^e = \alpha\mathbf{V}^e + Z(1 - \alpha)\mathbf{V}^m \quad (93)$$

and its part coming from EFIE is identical to Appendix B-A. The part $\hat{\mathbf{n}} \times \text{MFIE}$ however differs from MFIE from Appendix B-B. In particular, the excitation vector corresponding to incident magnetic field now reads

$$V_n^m = \int_{\Omega} (\hat{\mathbf{n}}(\mathbf{r}) \times \mathbf{H}^i(\mathbf{r})) \cdot \psi_n(\mathbf{r}) dS, \quad (94)$$

or equivalently,

$$j\mathbf{V}^m = -(\bar{\mathbf{U}}_1^T)^T \mathbf{a}, \quad (95)$$

with

$$\bar{\mathbf{U}}_1^n = \frac{k}{\sqrt{Z}} \left[\int_{\Omega} (\hat{\mathbf{n}}(\mathbf{r}) \times \mathbf{u}_{\alpha}^{(1)}(k\mathbf{r})) \cdot \psi_n(\mathbf{r}) dS \right]. \quad (96)$$

An algebraic relation between \mathbf{Z} and \mathbf{T} is given by

$$\mathbf{T} = -\mathbf{U}_1(\mathbf{Z}^{\text{ee}})^{-1}(\alpha\mathbf{U}_1 + jZ(1 - \alpha)\bar{\mathbf{U}}_1^n)^T. \quad (97)$$

Characteristic currents are in this case evaluated as

$$\mathbf{I}_n^e = t_n^{-1}(\mathbf{Z}^{\text{ee}})^{-1}(\alpha\mathbf{U}_1 + jZ(1 - \alpha)\bar{\mathbf{U}}_1^n)^T \mathbf{f}_n \quad (98)$$

which can also be transformed into a generalized eigenvalue problem

$$\mathbf{Z}^{\text{ee}}\mathbf{I}_n^e = (1 + j\lambda_n)(\alpha\mathbf{U}_1 + jZ(1 - \alpha)\bar{\mathbf{U}}_1^n)^T \mathbf{U}_1\mathbf{I}_n^e. \quad (99)$$

D. PMCHWT

The PMCHWT formulation for a homogeneous dielectric object can be considered as combining EFIE and MFIE in the interior and exterior regions

$$\mathbf{Z}_i\mathbf{I} = \begin{bmatrix} \mathbf{Z}_i^{\text{ee}} & j\mathbf{Z}_i^{\text{em}} \\ j\mathbf{Z}_i^{\text{me}} & \mathbf{Z}_i^{\text{mm}} \end{bmatrix} \begin{bmatrix} \mathbf{I}^e \\ j\mathbf{I}^m \end{bmatrix} = \begin{bmatrix} \mathbf{0} \\ \mathbf{0} \end{bmatrix} \quad (100)$$

and

$$\mathbf{Z}_o\mathbf{I} = \begin{bmatrix} \mathbf{Z}_o^{\text{ee}} & j\mathbf{Z}_o^{\text{em}} \\ j\mathbf{Z}_o^{\text{me}} & \mathbf{Z}_o^{\text{mm}} \end{bmatrix} \begin{bmatrix} \mathbf{I}^e \\ j\mathbf{I}^m \end{bmatrix} = \begin{bmatrix} \mathbf{V}^e \\ j\mathbf{V}^m \end{bmatrix} \quad (101)$$

where $\mathbf{Z}_{i/o}^{mn}$ is constructed by using the permittivity in the inner (i) and outer (o) region. The diagonal and off diagonal terms are determined by the EFIE (\mathcal{L}) and MFIE (\mathcal{K} and $\hat{\mathbf{n}} \times$, cf (84)) operators, respectively [19], [51]. Adding the matrices in (100) and (101) such that $\hat{\mathbf{n}} \times$ is eliminated defines the PMCHWT formulation. Here, it is noted that the radiation operator (37) is

$$\mathbf{R}_0 = \mathbf{U}^H\mathbf{U} = \text{Re}\{\mathbf{Z}_o\} \quad (102)$$

making (36) similar to the exterior formulation in [28].

APPENDIX C

INTERPOLATION BETWEEN UNITARY MATRICES

The interpolation (45)

$$\mathbf{F} = \mathbf{A}(\mathbf{A}^{-1}\mathbf{B})^\nu = \mathbf{A}\mathbf{C}^\nu, \quad \nu \in [0, 1] \quad (103)$$

is an interpolation between two unitary matrices \mathbf{A} and \mathbf{B} . Both matrices $\mathbf{C} = \mathbf{A}^{-1}\mathbf{B}$ and \mathbf{F} are also unitary, apparent from

$$\begin{aligned} \mathbf{C}^H\mathbf{C} &= \mathbf{B}^H\mathbf{A}^{-H}\mathbf{A}^{-1}\mathbf{B} = \mathbf{1} \\ \mathbf{F}^H\mathbf{F} &= (\mathbf{C}^\nu)^H\mathbf{A}^H\mathbf{A}\mathbf{C}^\nu = (\mathbf{C}^H)^\nu\mathbf{C}^\nu = (\mathbf{C}^H\mathbf{C})^\nu = \mathbf{1} \end{aligned} \quad (104)$$

In all cases, the matrix exponent is computed from a diagonalization

$$\mathbf{C}^\nu = (\mathbf{U}\mathbf{D}\mathbf{U}^H)^\nu = \mathbf{U}\mathbf{D}^\nu\mathbf{U}^H \quad (105)$$

with a diagonal matrix \mathbf{D} and a unitary matrix \mathbf{U} . The interpolation can also be expressed using the matrix exponent and matrix logarithm

$$\mathbf{C}^\nu = \exp(\nu \log(\mathbf{C})) \quad (106)$$

which highlights the connection with linear interpolation of the phase. This is clearly seen in the scalar case with $A = \exp(j\phi_a)$ and $B = \exp(j\phi_b)$ giving

$$F = A^{1-\nu}B^\nu = A(B/A)^\nu = e^{j(\phi_a(1-\nu) + \nu\phi_b)}. \quad (107)$$

APPENDIX D

SIMULTANEOUS DIAGONALIZATION OF THREE MATRICES

Diagonalization by Hermitian congruence [47]

$$\mathbf{X}^H(\mathbf{A} + j\mathbf{B})\mathbf{X} = \mathbf{D} \quad \text{and} \quad \mathbf{X}^H\mathbf{C}\mathbf{X} = \mathbf{1} \quad (108)$$

of three real symmetric matrices \mathbf{A} , \mathbf{B} , and \mathbf{C} is equivalent to simultaneous diagonalization of the three matrices. Here, \mathbf{D} denotes a diagonal matrix and, without loss of generality, \mathbf{X} is normalized according to the second diagonalization. Assume that $\mathbf{C} = \mathbf{U}^T\mathbf{U} = \mathbf{U}^H\mathbf{U}$ is positive definite and substitute the unitary matrix $\mathbf{Y} = \mathbf{U}\mathbf{X}$ into the first diagonalization

$$\mathbf{Y}^H(\mathbf{U}^{-H}(\mathbf{A} + j\mathbf{B})\mathbf{U}^{-1})\mathbf{Y} = \mathbf{D}. \quad (109)$$

Using that diagonalization with a unitary matrix is equivalent with normality [47] shows that

$$\mathbf{U}^{-H}(\mathbf{A} + j\mathbf{B})\mathbf{U}^{-1} \quad (110)$$

is normal matrix which reduces to a necessary and sufficient condition for simultaneous diagonalization of three matrices [68]

$$\mathbf{A}\mathbf{C}^{-1}\mathbf{B} = \mathbf{B}\mathbf{C}^{-1}\mathbf{A}. \quad (111)$$

The involved matrices can be permuted as long as they are invertible, see [68] for additional constraints for indefinite and singular matrices.

REFERENCES

- [1] R. J. Garbacz, "A generalized expansion for radiated and scattered fields," Ph.D. dissertation, The Ohio State Univ., 1968.
- [2] R. F. Harrington and J. R. Mautz, "Theory of characteristic modes for conducting bodies," *IEEE Trans. Antennas Propag.*, vol. 19, no. 5, pp. 622–628, Sept. 1971.
- [3] M. Cabedo-Fabres, E. Antonino-Daviu, A. Valero-Nogueira, and M. F. Bataller, "The theory of characteristic modes revisited: A contribution to the design of antennas for modern applications," *IEEE Antennas Propag. Mag.*, vol. 49, no. 5, pp. 52–68, Oct. 2007.
- [4] M. Vogel, G. Gampala, D. Ludick, U. Jakobus, and C. Reddy, "Characteristic mode analysis: Putting physics back into simulation," *IEEE Antennas Propag. Mag.*, vol. 57, no. 2, pp. 307–317, Apr. 2015.
- [5] Y. Chen and C.-F. Wang, *Characteristic Modes – Theory and Applications In Antenna Engineering*. Wiley, 2015.
- [6] P. Ylä-Oijala, "Generalized theory of characteristic modes," *IEEE Trans. Antennas Propag.*, vol. 67, no. 6, pp. 3915–3923, June 2019.
- [7] K. R. Schab, J. M. Outwater Jr., M. W. Young, and J. T. Bernhard, "Eigenvalue crossing avoidance in characteristic modes," *IEEE Trans. Antennas Propag.*, vol. 64, no. 7, pp. 2617–2627, July 2016.
- [8] A. O. Yee and R. J. Garbacz, "Self- and mutual-admittances of wire antennas in terms of characteristic modes," *IEEE Trans. Antennas Propag.*, vol. 21, no. 6, pp. 868–871, Nov. 1973.
- [9] M. Cabedo-Fabres, A. Valero-Nogueira, J. I. Herranz-Herruzo, and M. F. Bataller, "A discussion on the characteristic mode theory limitations and its improvement for the effective modeling of antennas and arrays," in *AP-S International Symposium*, vol. 1, June 2004, pp. 121–124.
- [10] C. G. Montgomery, R. H. Dicke, and E. M. Purcell, *Principles of Microwave Circuits*. New York, United States: McGraw-Hill, 1948.
- [11] R. J. Garbacz and R. H. Turpin, "A generalized expansion for radiated and scattered fields," *IEEE Trans. Antennas Propag.*, vol. 19, no. 3, pp. 348–358, May 1971.
- [12] G. Kristensson, *Scattering of Electromagnetic Waves by Obstacles*. Edison, NJ: SciTech Publishing, an imprint of the IET, 2016.
- [13] M. I. Mishchenko, L. D. Travis, and D. W. Mackowski, "T-matrix computations of light scattering by nonspherical particles: A review," *Journal of Quantitative Spectroscopy and Radiative Transfer*, vol. 55, no. 5, pp. 535 – 575, May 1996.
- [14] R. F. Harrington, "Antenna excitation for maximum gain," *IEEE Trans. Antennas Propag.*, vol. 13, no. 6, pp. 896–903, Nov. 1965.
- [15] —, *Field Computation by Moment Methods*. Piscataway, New Jersey, United States: Wiley – IEEE Press, 1993.
- [16] R. F. Harrington and J. R. Mautz, "Computation of characteristic modes for conducting bodies," *IEEE Trans. Antennas Propag.*, vol. 19, no. 5, pp. 629–639, Sept. 1971.
- [17] W. C. Gibson, *The Method of Moments in Electromagnetics*, 2nd ed. Chapman and Hall/CRC, 2014.
- [18] J. L. Volakis and K. Sertel, *Integral Equation Methods for Electromagnetics*. Scitech Publishing Inc., 2012.
- [19] W. C. Chew, M. S. Tong, and B. Hu, *Integral Equation Methods for Electromagnetic and Elastic Waves*. Morgan & Claypool, 2009.
- [20] J. J. H. Wang, *Generalized Moment Methods in Electromagnetics*. Wiley, 1991.
- [21] B. M. Kolundzija and A. R. Djordjevic, *Electromagnetic Modeling of Composite Metallic and Dielectric Structures*. Artech House, 2002.
- [22] D. Tayli, M. Capek, L. Akrou, V. Losenicky, L. Jelinek, and M. Gustafsson, "Accurate and efficient evaluation of characteristic modes," *IEEE Trans. Antennas Propag.*, vol. 66, no. 12, pp. 7066–7075, Dec. 2018.
- [23] A. F. Peterson, S. L. Ray, and R. Mittra, *Computational Methods for Electromagnetics*. Wiley – IEEE Press, 1998.
- [24] R. F. Harrington, J. R. Mautz, and Y. Chang, "Characteristic modes for dielectric and magnetic bodies," *IEEE Trans. Antennas Propag.*, vol. 20, no. 2, pp. 194–198, Mar. 1972.
- [25] A. J. Poggio and E. K. Miller, *Computer Techniques for Electromagnetics*. Pergamon, 1973.
- [26] T.-K. Wu and L. L. Tsai, "Scattering from arbitrarily-shaped lossy dielectric bodies of revolution," *Radio Science*, vol. 12, no. 5, pp. 709–718, 1977.
- [27] Y. Chang and R. F. Harrington, "A surface formulation for characteristic modes of material bodies," *IEEE Trans. Antennas Propag.*, vol. 25, no. 6, pp. 789–795, Nov. 1977.
- [28] P. Ylä-Oijala and H. Wallen, "PMCHWT-based characteristic mode formulations for material bodies," *IEEE Transactions on Antennas and Propagation*, vol. 68, no. 3, pp. 2158–2165, Mar. 2020.
- [29] M. Capek, P. Hazdra, P. Hamouz, and J. Eichler, "A method for tracking characteristic numbers and vectors," *Prog. Electromagn. Res. B*, vol. 33, pp. 115–134, 2011.
- [30] B. D. Raines and R. G. Rojas, "Wideband characteristic mode tracking," *IEEE Trans. Antennas Propag.*, vol. 60, no. 7, pp. 3537–3541, July 2012.
- [31] D. J. Ludick, U. Jakobus, and M. Vogel, "A tracking algorithm for the eigenvectors calculated with characteristic mode analysis," in *Proceedings of the 8th European Conference on Antennas and Propagation (EUCAP)*, 2014, pp. 569–572.
- [32] E. Safin and D. Manteuffel, "Advanced eigenvalue tracking of characteristic modes," *IEEE Trans. Antennas Propag.*, vol. 64, no. 7, pp. 2628–2636, July 2016.
- [33] M. Masek, M. Capek, L. Jelinek, and K. Schab, "Modal tracking based on group theory," *IEEE Trans. Antennas Propag.*, vol. 68, no. 2, pp. 927–937, Feb. 2020.
- [34] R. F. Harrington and J. R. Mautz, "Control of radar scattering by reactive loading," *IEEE Trans. Antennas Propag.*, vol. 20, no. 4, pp. 446–454, July 1972.
- [35] M. I. Mishchenko, "Comprehensive thematic T-matrix reference database: a 2017–2019 update," *Journal of Quantitative Spectroscopy and Radiative Transfer*, vol. 242, p. 106692, Feb. 2020.
- [36] V. L. Loke, T. A. Nieminen, N. R. Heckenberg, and H. Rubinsztein-Dunlop, "T-matrix calculation via discrete dipole approximation, point matching and exploiting symmetry," *Journal of Quantitative Spectroscopy and Radiative Transfer*, vol. 110, no. 14–16, pp. 1460–1471, 2009.
- [37] G. Demésey, J.-C. Auger, and B. Stout, "Scattering matrix of arbitrarily shaped objects: combining finite elements and vector partial waves," *JOŠA A*, vol. 35, no. 8, pp. 1401–1409, 2018.
- [38] M. Fruhnert, I. Fernandez-Corbaton, V. Yannopapas, and C. Rockstuhl, "Computing the T-matrix of a scattering object with multiple plane wave illuminations," *Beilstein journal of nanotechnology*, vol. 8, no. 1, pp. 614–626, 2017.
- [39] V. L. Loke, T. A. Nieminen, S. J. Parkin, N. R. Heckenberg, and H. Rubinsztein-Dunlop, "FDFD/T-matrix hybrid method," *Journal of Quantitative Spectroscopy and Radiative Transfer*, vol. 106, no. 1–3, pp. 274–284, 2007.
- [40] J. A. Stratton, *Electromagnetic Theory*. Wiley – IEEE Press, 2007.
- [41] C. A. Balanis, *Advanced Engineering Electromagnetics*. Wiley, 1989.
- [42] A. Zangwill, *Modern Electrodynamics*. Cambridge University Press, 2012.
- [43] J. E. Hansen, Ed., *Spherical Near-Field Antenna Measurements*. United Kingdom: The Institution of Engineering and Technology, 2008.

- [44] B. A. Austin and K. P. Murray, "The application of characteristic-mode techniques to vehicle-mounted NVIS antennas," *IEEE Antennas Propag. Mag.*, vol. 40, pp. 7–21, Feb. 1998.
- [45] R. E. Collin, *Foundations for Microwave Engineering*, 2nd ed. Wiley – IEEE Press, 1992.
- [46] E. Newman, "Small antenna location synthesis using characteristic modes," *IEEE Trans. Antennas Propag.*, vol. 27, no. 4, pp. 530–531, July 1979.
- [47] R. A. Horn and C. R. Johnson, *Matrix Analysis*. Cambridge, United Kingdom: Cambridge University Press, 2017.
- [48] P. C. Waterman, "Matrix formulation of electromagnetic scattering," *Proceedings of the IEEE*, vol. 53, no. 8, pp. 805 – 812, Aug. 1965.
- [49] S. Huang, J. Pan, C.-F. Wang, Y. Luo, and D. Yang, "Unified implementation and cross-validation of the integral equation-based formulations for the characteristic modes of dielectric bodies," *IEEE Access*, vol. 8, pp. 5655–5666, 2019.
- [50] F.-G. Hu and C.-F. Wang, "Integral equation formulations for characteristic modes of dielectric and magnetic bodies," *IEEE Transactions on Antennas and Propagation*, vol. 64, no. 11, pp. 4770–4776, 2016.
- [51] J.-M. Jin, *Theory and Computation of Electromagnetic Fields*. Wiley, 2010.
- [52] M. I. Mishchenko, J. W. Hovenier, and L. D. Travis, *Light scattering by nonspherical particles: theory, measurements, and applications*. IOP Publishing, 2000.
- [53] L. Gurel and W. C. Chew, "On the connection of T matrices and integral equations," in *Antennas and Propagation Society Symposium 1991 Digest*. IEEE, 1991.
- [54] K. T. Kim and B. A. Kramer, "Direct determination of the T-Matrix from a MoM impedance matrix computed using the Rao-Wilton-Glisson basis function," *IEEE Transactions on Antennas and Propagation*, vol. 61, no. 10, pp. 5324–5327, Oct. 2013.
- [55] J. Markkanen and A. J. Yuffa, "Fast superposition T-matrix solution for clusters with arbitrarily-shaped constituent particles," *Journal of Quantitative Spectroscopy and Radiative Transfer*, vol. 189, pp. 181–188, Mar. 2017.
- [56] V. Losenicky, L. Jelinek, M. Capek, and M. Gustafsson, "Method of moments and T-matrix hybrid," *arXiv preprint arXiv: 2012.04303*, 2021. [Online]. Available: <https://arxiv.org/abs/2012.04303>
- [57] T. Nieminen, H. Rubinsztein-Dunlop, and N. Heckenberg, "Calculation of the T-matrix: general considerations and application of the point-matching method," *Journal of Quantitative Spectroscopy and Radiative Transfer*, vol. 79, pp. 1019–1029, 2003.
- [58] H. Reid, *Electromagnetism in the Spherical-Wave Basis*, SCUFF-EM documentation, 2016.
- [59] Z. Miers and B. K. Lau, "Wide band characteristic mode tracking utilizing far-field patterns," *IEEE Antennas Wireless Propag. Lett.*, vol. 14, pp. 1658–1661, 2015.
- [60] X. J. Chen, Y. M. Pan, and G. D. Su, "An advanced eigenvector-correlation-based tracking method for characteristic modes," *IEEE Transactions on Antennas and Propagation*, vol. 69, no. 5, pp. 2751–2758, May 2021.
- [61] K. R. Schab and J. T. Bernhard, "A group theory rule for predicting eigenvalue crossings in characteristic mode analyses," *IEEE Antennas Wireless Propag. Lett.*, no. 16, pp. 944–947, 2017.
- [62] P. Delsarte, Y. Genin, and Y. Kamp, "On the role of the Nevanlinna–Pick problem in circuit and system theory," *International Journal of Circuit Theory and Applications*, vol. 9, no. 2, pp. 177–187, 1981.
- [63] B. Gustavsen and A. Semlyen, "Rational approximation of frequency domain responses by vector fitting," *IEEE Trans. Power Delivery*, vol. 14, pp. 1052–1061, 1999.
- [64] A. Bernland, M. Gustafsson, and S. Nordebo, "Physical limitations on the scattering of electromagnetic vector spherical waves," *Journal of Physics A: Mathematical and Theoretical*, vol. 44, no. 145401, pp. 1–21, 2011.
- [65] M. Gustafsson, "On the non-uniqueness of the electromagnetic instantaneous response," *J. Phys. A: Math. Gen.*, vol. 36, pp. 1743–1758, 2003.
- [66] R. G. Vaughan and J. B. Andersen, "Antenna diversity in mobile communications," *IEEE Transactions on Vehicular Technology*, vol. 36, no. 4, pp. 149–172, 11 1987.
- [67] J. Thaysen and K. B. Jakobsen, "Envelope correlation in (n, n) mimo antenna array from scattering parameters," *Microwave and optical technology letters*, vol. 48, no. 5, pp. 832–834, 2006.
- [68] M. A. Novikov, "Simultaneous diagonalization of three real symmetric matrices," *Russian Mathematics*, vol. 58, no. 12, pp. 59–69, 2014.
- [69] M. Gustafsson, M. Capek, and K. Schab, "Tradeoff between antenna efficiency and Q-factor," *IEEE Trans. Antennas Propag.*, vol. 67, no. 4, pp. 2482–2493, April 2019.
- [70] P. M. Morse and H. Feshbach, *Methods of Theoretical Physics*. McGraw-Hill, 1953.
- [71] M. Capek, V. Losenicky, L. Jelinek, and M. Gustafsson, "Validating the characteristic modes solvers," *IEEE Trans. Antennas Propag.*, vol. 65, no. 8, pp. 4134–4145, Aug. 2017.
- [72] R. McWeeny, *Symmetry: An Introduction to Group Theory and Its Applications*. London: Pergamon Press, 1963.
- [73] J. Song and W. C. Chew, "Error analysis for the truncation of multipole expansion of vector green's functions [EM scattering]," *IEEE Microwave and Wireless Components Letters*, vol. 11, no. 7, pp. 311–313, Jul. 2001. [Online]. Available: <https://doi.org/10.1109/7260.933781>
- [74] J. R. Mautz and R. F. Harrington, "Radiation and scattering from bodies of revolution," *Applied Scientific Research*, vol. 20, no. 1, pp. 405–435, Jan. 1969.
- [75] P. Ylä-Oijala, H. Wallén, D. Tzarouchis, and A. Sihvola, "Surface integral equation-based characteristic mode formulation for penetrable bodies," *IEEE Trans. Antennas Propag.*, vol. 66, no. 7, pp. 3532–3539, July 2018.
- [76] H. Akima, "A new method of interpolation and smooth curve fitting based on local procedures," *Journal of the ACM (JACM)*, vol. 17, no. 4, pp. 589–602, 1970.
- [77] J. von Neumann and E. Wigner, *On the Behaviour of Eigenvalues in Adiabatic Processes*. Singapore: World Scientific, 2000.
- [78] T. K. Sarkar, E. L. Mokole, and M. Salazar-Palma, "An expose on internal resonance, external resonance and characteristic modes," *IEEE Trans. Antennas Propag.*, vol. 64, no. 11, pp. 4695–4702, Nov. 2016.
- [79] M. Capek, L. Jelinek, and M. Masek, "Finding optimal total active reflection coefficient and realized gain for multi-port lossy antennas," *IEEE Trans. Antennas Propag.*, 2021, early access.
- [80] J. Mautz and R. Harrington, "Modal analysis of loaded N-port scatterers," *IEEE Trans. Antennas Propag.*, vol. 21, no. 2, pp. 188–199, Mar. 1973.
- [81] J. L. T. Ethier and D. McNamara, "Sub-structure characteristic mode concept for antenna shape synthesis," *Electron. Lett.*, vol. 48, no. 9, pp. 471–472, Apr. 2012.
- [82] P. Ylä-Oijala and H. Wallén, "Theory of characteristic modes for nonsymmetric surface integral operators," *IEEE Transactions on Antennas and Propagation*, vol. 69, no. 3, pp. 1505–1512, 2021. [Online]. Available: <https://doi.org/10.1109/tap.2020.3017437>
- [83] N. Inagaki and R. J. Garbacz, "Eigenfunctions of composite hermitian operators with application to discrete and continuous radiating systems," *IEEE Trans. Antennas Propag.*, vol. 30, no. 4, pp. 571–575, July 1982.
- [84] K. Schab, "Modal analysis of radiation and energy storage mechanisms on conducting scatterers," Ph.D. dissertation, University of Illinois at Urbana-Champaign, 2016.
- [85] M. Gustafsson, K. Schab, L. Jelinek, and M. Capek, "Upper bounds on absorption and scattering," *New Journal of Physics*, vol. 22, p. 073013, 2020.
- [86] J. D. Jackson, *Classical Electrodynamics*, 3rd ed. Wiley, 1998.
- [87] F. Zhang, *Matrix theory: basic results and techniques*. Springer Science & Business Media, 2011.
- [88] T. B. A. Senior and J. L. Volakis, *Approximate Boundary Conditions in Electromagnetics*. IEE, 1995.
- [89] Q. I. Dai, Q. S. Liu, H. U. I. Gan, and W. C. Chew, "Combined field integral equation-based theory of characteristic mode," *IEEE Trans. Antennas Propag.*, vol. 63, no. 9, pp. 3973–3981, Sept. 2016.
- [90] R. F. Harrington and J. R. Mautz, "H-field, E-field and combined-field solutions for conducting bodies of revolution," *RADC-TR-77-109 Interim Technical Report*, pp. 1–45, 1977.



Mats Gustafsson received the M.Sc. degree in Engineering Physics 1994, the Ph.D. degree in Electromagnetic Theory 2000, was appointed Docent 2005, and Professor of Electromagnetic Theory 2011, all from Lund University, Sweden.

He co-founded the company Phase holographic imaging AB in 2004. His research interests are in scattering and antenna theory and inverse scattering and imaging. He has written over 100 peer reviewed journal papers and over 100 conference papers. Prof.

Gustafsson received the IEEE Schelkunoff Transactions Prize Paper Award 2010, the IEEE Uslenghi Letters Prize Paper Award 2019, and best paper awards at EuCAP 2007 and 2013. He served as an IEEE AP-S Distinguished Lecturer for 2013-15.



Lukas Jelinek received his Ph.D. degree from the Czech Technical University in Prague, Czech Republic, in 2006. In 2015 he was appointed Associate Professor at the Department of Electromagnetic Field at the same university.

His research interests include wave propagation in complex media, electromagnetic field theory, metamaterials, numerical techniques, and optimization.



Kurt Schab (M'16) Kurt Schab is an Assistant Professor of Electrical Engineering at Santa Clara University, Santa Clara, CA USA. He received the B.S. degree in electrical engineering and physics from Portland State University in 2011, and the M.S. and Ph.D. degrees in electrical engineering from the University of Illinois at Urbana-Champaign in 2013 and 2016, respectively. From 2016 to 2018 he was an Intelligence Community Postdoctoral Research Scholar at North Carolina State University in Raleigh, North Carolina. His research focuses on

the intersection of numerical methods, electromagnetic theory, and antenna design.



Miloslav Capek (M'14, SM'17) received the M.Sc. degree in Electrical Engineering 2009, the Ph.D. degree in 2014, and was appointed Associate Professor in 2017, all from the Czech Technical University in Prague, Czech Republic.

He leads the development of the AToM (Antenna Toolbox for Matlab) package. His research interests are in the area of electromagnetic theory, electrically small antennas, numerical techniques, and optimization. He authored or co-authored over 100 journal and conference papers.

Dr. Capek is member of Radioengineering Society and Associate Editor of IET Microwaves, Antennas & Propagation.